CO4-1   Effect on the Switch of the Helicity of Poly(quinoxaline-2,3-diyl)s: A Structural Analysis by Small-Angle X-ray Scattering

Y. Nagata, M. Suginome, M. Sugiyama[1], R. Inoue[1] and N. Sato[1]

Graduate School of Science, Kyoto University
[1] *Institute for Integrated Radiation and Nuclear Science, Kyoto University*

INTRODUCTION: Helix is one of the simplest chiral motifs, being widely found in natural biomacromolecules, including DNA, RNA, proteins, and polysaccharides. Increasing attention has been paid to the structural control of artificial helical polymers because of their scientific and industrial applications for asymmetric catalysts, chiral stationary phase, and chiroptical materials. So far, we reported that single-handed helical poly(quinoxaline-2,3-diyl)s (PQXs) bearing chiral side chains exhibit solvent-dependent helix inversion,[1,2] which can serve as effective scaffold for chirality-switchable catalysts[3-7] and chiroptical materials.[8-11] For example, a PQX bearing chiral (*R*)-2-octyloxymethyl side chains (**2oct**) adopts right- or left-handed helical structures in tetrahydrofuran (THF) or 1,1,2-trichloroethane (1,1,2-TCE), respectively (Figure 1). It should be noted that the PQXs can exhibit a perfect solvent-dependent helix inversion between left-handed (>99%) to right-handed (>99%) structures, which is an unprecedented feature among various helical polymers. Therefore, it is urgent and essential issue to reveal the mechanism of the solvent-dependent helix inversion of the PQX for the development of advanced functional chiral materials. Furthermore, the solvent-dependent helix inversion can be a good educational example to understand the behavior of macromolecules. However, the detailed mechanism has been still unclear at this stage. In this study, we tried to reveal the detailed structure of **2oct** in solution by using small-angle X-ray scattering (SAXS) measurements.[12]
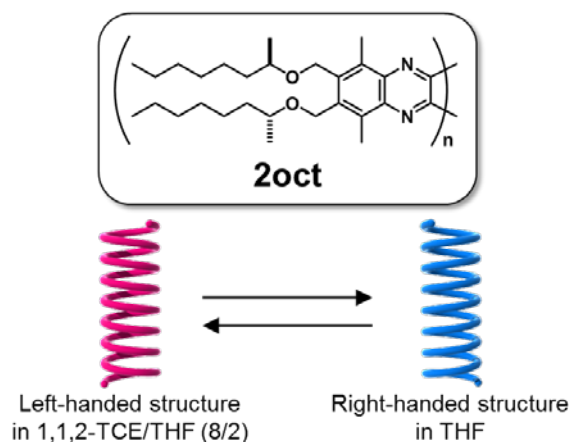

Figure 1. Structure of 2oct exhibiting the solvent-dependent helix inversion

EXPERIMENTS and RESULTS: **2oct** was dissolved in tetrahydrofuran to measure the SAXS patterns by using the Rigaku NANOPIX SAXS/WAXS measurement system (Figure 2). Now we are trying to elucidate the detailed structure of **2oct** in solution from the SAXS pattern along with the theoretical calculations.
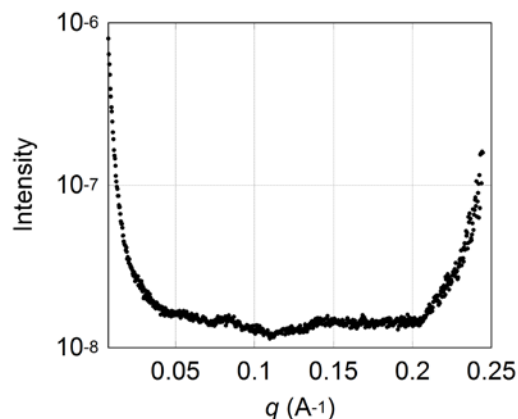

Figure 2. SAXS pattern of **2oct** dissolved in tetrahydrofuran.

REFERENCES:
(1) Yamada, T.; Nagata, Y.; Suginome, M. *Chem. Commun.* 46 (2010) 4914-4916.
(2) Nagata, Y.; Yamada, T.; Adachi, T.; Akai, Y.; Yamamoto, T.; Suginome, M. *J. Am. Chem. Soc.*, *135* (2013) 10104-10113.
(3) Yamamoto, T.; Yamada, T.; Nagata, Y.; Suginome, M. *J. Am. Chem. Soc.*, *132* (2010) 7899-7901.
(4) Nagata, Y.; Kuroda, T.; Takagi, K.; Suginome, M. *Chem. Sci.*, **5** (2014) 4953-4956.
(5) Nagata, Y.; Nishikawa, T.; Suginome, M. *J. Am. Chem. Soc.,* **136** (2014) 15901-15904.
(6) Ke, Y.-Z.; Nagata, Y.; Yamada, T.; Suginome, M. *Angew. Chem. Int. Ed.,* **54** (2015) 9333-9337.
(7) Nagata, Y.; Nishikawa, T.; Suginome, M. *ACS Macro Lett.,* **5** (2016) 519-522.
(8) Nagata, Y.; Nishikawa, T.; Suginome, M. *Chem. Commun.,* **50** (2014) 9951-9953.
(9) Nagata, Y.; Takagi, K.; Suginome, M. *J. Am. Chem. Soc.,* **136** (2014) 9858-9861.
(10) Nagata, Y.; Uno, M.; Suginome, M. *Angew. Chem. Int. Ed.,* **55** (2016) 7126-7130.
(11) Nishikawa, T.; Nagata, Y.; Suginome, M. *ACS Macro Lett.,* **6** (2017) 431-435.
(12) For SANS experiments; Nagata, Y.; Nishikawa, T.; Suginome, M.; Sato, S.; Sugiyama, M.; Porcar, L.; Mar-tel, A.; Inoue, R.; Sato, N. *J. Am. Chem. Soc.*, **140** (2018) 2722-2726.

Nanostructures in Semiconductor Nanocomposite Thin Films

Y. Oba, S. Abe[1] and M. Sugiyama[2]

Materials sciences Research Center, Japan Atomic Energy Agency
[1]*Research Institute for Electromagnetic Materials*
[2]*Institute for Integrated Radiation and Nuclear Science, Kyoto University*

INTRODUCTION: Semiconductor nanocomposite thin films have attracted much attention due to their potential to quantum-dot solar cells [1,2]. They consist semiconductor nanocrystals embedded in the matrix of another semiconductor. The nanocrystals induce the quantum size effects and enhance conversion efficiency [3,4]. In addition, the semiconductor nanocomposite thin films can utilize a wide range of the solar spectrum for energy conversion because of the difference in the band gap between the nanocrystals and the matrix.

  Since the quantum size effects are highly related to the size of the nanocrystals, the characterization and control of the size of the nanocrystals are crucial to develop high-efficiency materials. For the characterization of the nanostructures, small-angle X-ray scattering (SAXS) is a powerful means. Therefore, the SAXS measurements of the semiconductor nanocomposite thin films were performed.

EXPERIMENTS: The nanocomposite thin films were deposited on Si substrates by one-step synthesis techniques [1]. The nanocrystals are precipitated in the films during deposition. The thickness of the films and the substrates were around 1 µm and 0.5 mm. SAXS measurements were performed using a SAXS instrument with Mo Kα radiation (Nano-viewer, RIGAKU) installed at the Institute for Integrated Radiation and Nuclear Science, Kyoto University. The characteristic X-ray emitted from Mo (17 keV) can penetrate the thicker substrates compared to that from Cu. The SAXS profiles were measured with two sample-to-detector distances of 45 and 160 cm to cover a wide q range. Here, q is the magnitude of the scattering vector and is equal to $(4\pi/\lambda)\sin\theta$, where θ and λ are half the scattering angle and the wavelength of the incident X-ray. During the SAXS measurements, the samples were put in vacuum to reduce the background scattering from air. The glassy carbon standard provided by the Argonne National Laboratory was used to calibrate the scattering intensity [5].

RESULTS: Fig. 1 shows a typical SAXS profile of the semiconductor nanocomposite thin film composed of the
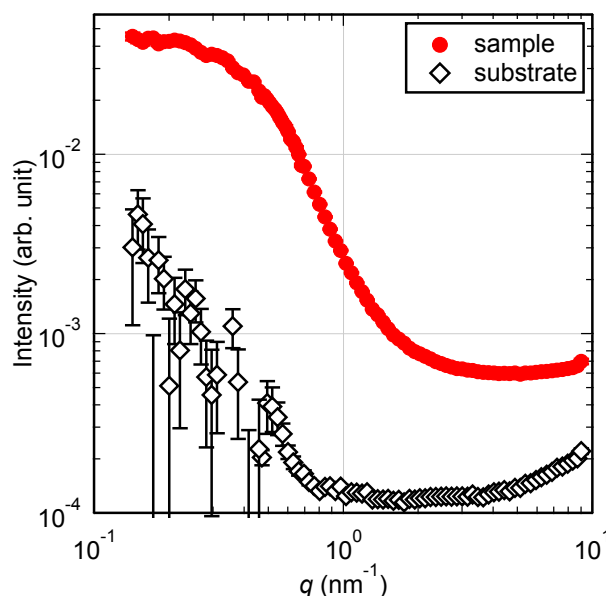

Fig. 1. SAXS profiles of a semiconductor nanocomposite thin film and a Si substrate.

PbTe nanocrystals and the ZnSe matrix [1]. The SAXS profile of the Si substrate is also shown in Fig. 1 for comparison. The SAXS profile of the sample shows a shoulder around q=0.5 nm^{-1}. This indicates that the nanostructures are formed in the film. The diameter of the nanocrystals is estimated to be around a few nm using the Guinier plot [6]. Since the exciton Bohr radius of PbTe is 150 nm [7], the observed nanocrystals are small enough to induce the quantum size effects.

REFERENCES:
[1] S. Abe, Mater. Renew. Sustain. Energy, **4** (2015) 18/1-7.
[2] V. Arivazhagan *et al.*, Appl. Phys. Lett., **102** (2013) 242110/1-4.
[3] A. Nozik, Physica E, **14** (2002) 115-120.
[4] M. Grätzel, Inorg. Chem., **44** (2005) 6841-6851.
[5] F. Zhang *et al.*, Metal. Mater. Trans. A, **41A** (2010) 1151-1158.
[6] L. A. Feigin, *Structure Analysis by Small-Angle X-Ray and Neutron Scattering*, (Plenum Press, New York,1987).
[7] J. E. Murphy *et al.*, J. Am. Chem. Soc., **128** (2006) 3241-3247.

Measurement of Electron Emission Properties of Field Emitter Array under Gamma-ray Irradiation

Y. Gotoh, T. Morito, Y. Handa, M. Nagao[1], T. Okamoto[2], N. Sato[3], M. Akiyoshi[4], and I. Takagi

Graduate School of Science, Kyoto University
[1]National Institute of Advanced Industrial Science and Technology
[2]National Institute of Technology, Kisarazu College,
[3]Institute for Integrated Radiation and Nuclear Science, Kyoto University
[4]Radiation Research Center, Osaka Prefecture University

INTRODUCTION: Taking advantage of the high durability of vacuum electronic devices, we are developing a radiation tolerant compact image sensor with field emitter array [1]. In order to show the sufficient tolerance against gamma-ray irradiation, it is necessary to measure the performance of the device in radiation field. Especially, operation of field emitter array (FEA), which is the electron source of this device, should be confirmed to assure the performance of the image sensor. Since the FEA is operated in vacuum, it is necessary to develop a vacuum container which can maintain the interior pressure under 10^{-6} Pa. We have already reported the results of the preliminary experiments last year [2]. This year, non-evaporation getter (NEG) pump was attached to the vessel. In this report, we will describe the pressure in the vessel after encapsulating, and also the results of the measurement of electron emission properties of the FEA.

EXPERIMENTS: A vacuum vessel was prepared for the measurement of the electron emission properties of FEAs under the gamma-ray irradiation. The vessel had four ports: the ports were for a NEG pump, an all metal angle valve, glass tube in which the FEA is settled, and flange for the voltage and current inlet. Prior to the measurement, we have settled a vacuum gauge instead of the FEA in order to evaluate the attainable vacuum pressure inside the vessel. After pumping and activating the NEG pump (pumping speed of 100 L s^{-1} for hydrogen), the vessel could reach less than 10^{-7} Pa. Then a sample on which a dozen FEAs were mounted was installed in the vessel. The FEA measured in the present study was a single gate Spindt-type FEA with 1000 emission tips. Above the FEA, an anode electrode made of stainless steel, was positioned. The current-voltage (*I-V*) characteristics of the FEA were measured before, during, and after the gamma-ray irradiation to the FEA. A positive voltage of 200 V was given to the anode, and a negative lamp voltage to -70 V was applied to the emitter. The gate was grounded. The gamma-ray irradiation was performed at Co-60 Gamma-ray Irradiation Facility, Institute for Integrated Radiation and Nuclear Science, Kyoto University. The dose rate of irradiation was about 1 kGy h^{-1}. The irradiation continued for half an hour, and the *I-V* measurements were done every 5 min. After this series of the measurement, the vacuum vessel was kept for several weeks. The pressure inside the vessel was examined from the pressure variation of another vacuum chamber to which the test tube was connected.

RESULTS: Throughout the experiments, the FEA showed a good electron emission properties and no serious deterioration was observed. Figure 1 shows the *I-V* characteristics before, during, and after the gamma-ray irradiation. The *I-V* curve obtained after the gamma-ray irradiation (red line) overlaps the curve obtained before the gamma-ray irradiation (black line). Constant current observed at the lower gate-emitter voltage is due to the leakage current because the anode was at a high voltage of 200 V. During the gamma-ray irradiation, the *I-V* curves showed little difference with those without irradiation. At a lower voltage, the leakage current increased (blue line). This would be probably due to the incident of electrons from glass tube or other part of the system under the gamma-ray irradiation. These results show that the FEA has tolerance against gamma-ray irradiation. It was found that the vacuum vessel maintained sufficient low pressure even after 2 month. More 2 month later, the FEA could be operated stably, which implies that the pressure inside the vessel was sufficiently low. It was found that the present system can evaluate the tolerance of the FEAs relatively long time.
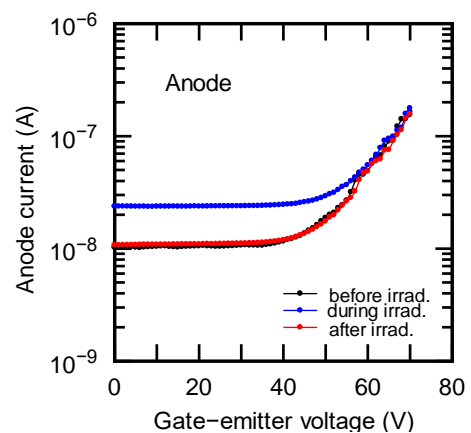

Fig. 1. Current-voltage characteristics of the FEA before and after the gamma-ray irradiation.

REFERENCES:
[1] Y. Gotoh *et al.*, 2017 IEEE 30th International Vacuum Nanoelectronics Conference (2017) 104.
[2] Y. Gotoh *et al.*, KURRI Progress Report 2016 (2017).

CO4-4 Evaluation of Unintentionally Doped Impurities in Sillicon Carbide Substrates using Nutron Activation Analysis Technics

T. Makino, H. Yashima[1], S. Sekimoto[1] and T. Ohshima

Quantum Beam Science Research Directorate, National Institutes for Quantum and Radiological Science and Technology

[1]*Kyoto Univ.*

INTRODUCTION: Silicon carbide(SiC) is regarded as a promising candidate for high power and high frequency electronic devices. For the high-performance device fabrication, it is necessary to develop the fabrication process of high quality substrates with low impurity content. However, unintentionally impurity of SiC in substrate have not been estimated quantitatively [1]. Therefore, we evaluated unintentionally doped impurities in SiC wafers by using neutron activation analysis technics.

EXPERIMENTS: Commercially available two pol types of SiC substrate (4H-SiC and 3C-SiC) were used for the evaluation. Moreover, two 4H-SiC substrates grown by different company were prepared (4H-SiC: A, 4H-SiC: B). Substrates were cut into 5 mm x 10 mm, and cleaning acetone with ultrasonic for 10 min. After the organic cleaning, samples were cleaned by nitro-hydrochloric acid (HCl:HNO_3=3:1) for 5 min. followed by hydrofluoric acid (50% HF) for 5min. Between the each treatment, samples were rinsed by de-ionized H_2O. To quantitative estimation of impunities, standard sample were prepared by using metallic solutions known contents of metals. These samples and standard samples were capsuled with polyethylene packs.

Capsuled samples were irradiated by neutrons for 1 hour at the KUR with 1MW. After the irradiation, gamma-ray spectra from activated impurity in substrate and standard samples were measured with high-purity Ge detectors.

RESULTS: Table 1 shows observed impurity nuclides and the order of concentrations. From 4H-SiC wafers, sodium, manganese, bromine, tungsten, were detected with the concentration of $10^{14} \sim 10^{15}$ /cm^3. For 3C-SiC, arsenide was detected with the concentration of 10^{14} /cm^3 additionally, while tungsten was not detected.

CONCLUSION: We obtained clear poly-type dependence of unintentionally doped impurities on SiC substrates. Moreover, slight deference was observed for concentration of some impurities for 4H-SiCs.

In future, we will carefully analyze the quantitative values of the concentration, and effects of the impurities for electric devices fabricated by the SiCs.

Table 1. Observed impurity nuclides and the order of concentrations from SiCs

Nuclide	Concentration [/cm^3]		
	4H-SiC: A	4H-SiC: B	3C-SiC
Na	3×10^{15}	4×10^{15}	3×10^{15}
Mn	1×10^{14}	8×10^{14}	5×10^{14}
As	ND	ND	2×10^{14}
Br	2×10^{14}	2×10^{15}	4×10^{14}
W	9×10^{14}	3×10^{15}	ND

REFERENCE:
[1] T. Ohshima *et al.,* Matt. Sci. Forum Vol. 556-557, 457-460.

Spectrum of Amino Acid in the Millimeter-wave Region using a Diode Detector

T. Takahashi

Institute for Integrated Radiation and Nuclear Science, Kyoto University

INTRODUCTION: In recent years various types of coherent radiation emitted from a short bunch of relativistic electrons have attracted a considerable attention as a bright light source in the THz-wave and millimeter wave regions for the spectroscopic purpose. Coherent transition radiation (CTR), which is emitted from a boundary between two media, is one of such a coherent light source. CTR is usually utilized as a non-polarized light source, because the electric vector of transition radiation (TR) emitted from a metallic screen is axially symmetric with respect to the trajectory of an electron beam. The new system of the circularly polarized CTR using a pair of wire-grid radiators with the different polarization has been developed [1]. The significant point of my new technique is the use of linearly polarized CTR with the wire-grid radiator. With this technique the polarization degree is able to be controlled precisely. Circularly polarized light has been useful in the circular dichroism spectroscopy. In the previous report [2] spectra of some kinds of amino acid have been measured using linearly polarized CTR with a conventional bolometer over the wide wavelength range. In this report spectra in the millimeter-wave region has been investigated in detail with a diode detector.

EXPERIMENTAL PROCEDURES: The experiment was performed at the coherent radiation beamline [3] at the L-band linac of the Institute for Integrated Radiation and Nuclear Science, Kyoto University. The energy, the width of the macro pulse, and the repetition rate of the electron beam were 42 MeV, 100 ns, and 60 Hz, respectively. The average current of the electron beam was 3.5 μA. The spectrum of CTR was measured by a Martin-Puplett type inter- ferometer and a diode detector (DPX-10, Millitec Inc.) with a boxcar integrator. The schematic diagram of the experiment was shown in Fig.1.

RESULTS: Measured spectra of some kinds of amino acid, e.g., Phenylalanine, α-Alanine, and Tryptophan, are shown in Figs. 2. The identification of observed absorption is now in progress

REFERENCES:

[1] T. Takahashi, *et al.*, KURRI-PR 2015 CO4-7.
[2] T. Takahashi, *et al.*, KURRI-PR 2016 CO4-8.
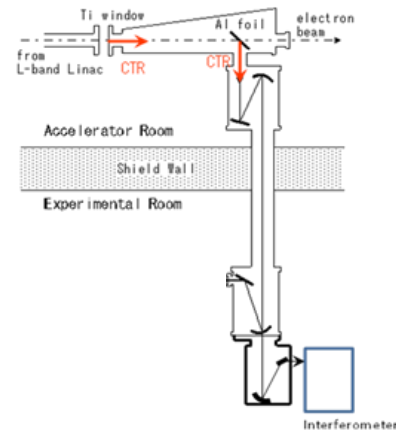[3] T. Takahashi *et al.*, Rev. Sci. Instrum. **69** (1998) 3770.
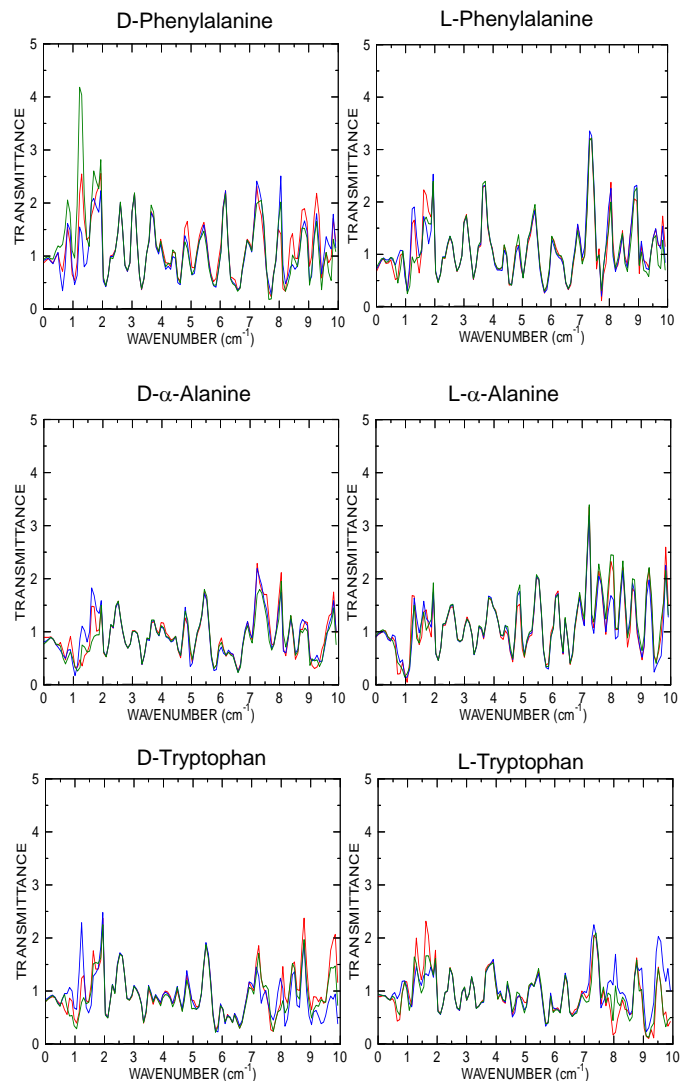
Fig.1 The schematic diagram of the experiment.

Fig.2 Spectra of some kinds of amino acid.

CO4-6 Correlation between Neutron Irradiation Damages and Hydrogen Isotope Retention

Y. Oya, A. Togari[1], M. Nakata[1], M. Zhao[1], Y. Iinuma[2] and R. Okumura[2]

Faculty of Science, Shizuoka University,
[1]Graduate School of Science, Shizuoka University
[2]Research Reactor Institute, Kyoto University

INTRODUCTION: Li-based ceramic is one of the promising candidates for the tritium breeding materials in the D-T fusion reactor. Tritium is expected to be produced by the irradiation of neutron on Li atom to achieve the self-sustenance of D-T fusion reaction. It is important to understand the tritium breeding and desorption processes from the viewpoint of steady recovery of tritium. Recently, advanced composites such as Li_2TiO_3-Li_4SiO_4 materials are proposed [1] to combine the good chemical stability of Li_2TiO_3 and preferable tritium release property of Li_4SiO_4. However, the neutron irradiation behavior and subsequent tritium release data on this new materials are scarce. In this study, neutron irradiation on the composite Li_2TiO_3- Li_4SiO_4 materials was carried out at KUR, and tritium release behavior was evaluated by thermal desorption spectroscopy (TDS) and liquid scintillation counter (LSC) measurement.

EXPERIMENTS: Composite Li_2TiO_3-Li_4SiO_4 with the Ti/Si ratio of 2.0 and 0.5, pure Li_2TiO_3, and pure Li_4SiO_4 powders were prepared by solution combustion synthesis. The crystallite size of the powders is around 50 nm. The as-synthesized powders were annealed at 923 K for 2h at ambient atmosphere to remove the carbon and impurities. Thereafter, neutron irradiation on the samples was performed using the pneumatic tubes 2 (Pn-2) at KUR [2]. The thermal neutron flux was 2.75×10^{13} n cm^{-2} s^{-1} and fluence was 9.9×10^{16} n cm^{-2}. After irradiation, the samples were transferred to Shizuoka University to perform the tritium-TDS and LSC measurement.

RESULTS: Fig. 1 shows the tritium-TDS spectra of the neutron-irradiated samples with the heating rate of 30 K min^{-1}. Tritium is released at the temperature range of 400-1000 K. The pure Li_2TiO_3 shows a major desorption peak at 580 K and a sub-peak at around 680 K. The pure Li_4SiO_4 shows 4 peaks at different temperatures and it is noticed that compared with Li_2TiO_3 the tritium desorption starts at the lower temperature of 400 K. For the composite Ti/Si=2.0, tritium desorption started at 400 K which was also lower than that for pure Li_2TiO_3, indicating that Li_4SiO_4 crystallites embedded in Li_2TiO_3 facilitated the tritium release from Li_2TiO_3 at lower temperature possibly due to high Li atom density in Li_4SiO_4 grains. For the composite Ti/Si=0.5, most tritium released at lower temperature below 600 K compared with pure Li_4SiO_4. Fig. 2 shows tritium-TDS spectra of composite Ti/Si=2.0 at different heating rates. The tritium desorption was shifted toward lower temperature side by decreasing heating rate. Three desorption peaks can be separated and activation energies for these peaks were obtained through the Arrhenius plot based on the peak shifting. For Peaks 1, 2 and 3, the activation energies were calculated to be 0.18, 0.20, 0.27 eV respectively, which were much lower than the conventional single phase breeders. It can be concluded that composite Li_2TiO_3-Li_4SiO_4 breeders combine the steady chemical stability of Li_2TiO_3 and enhanced tritium release behavior at lower temperature with decreased activation energy.
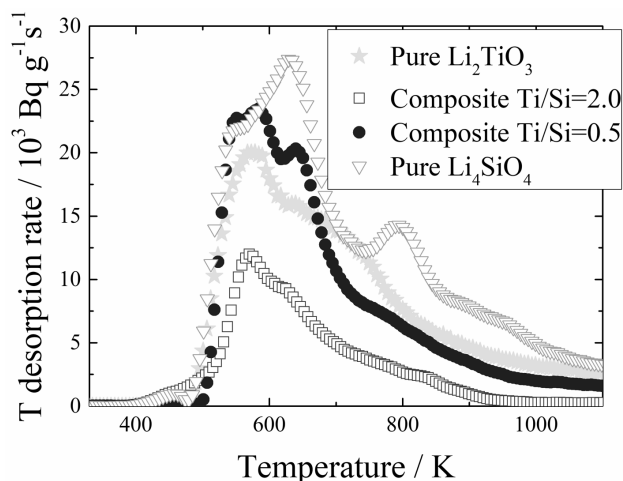

Fig. 1. Tritium-TDS spectra of the neutron irradiated materials with the heating of 30 K min^{-1}
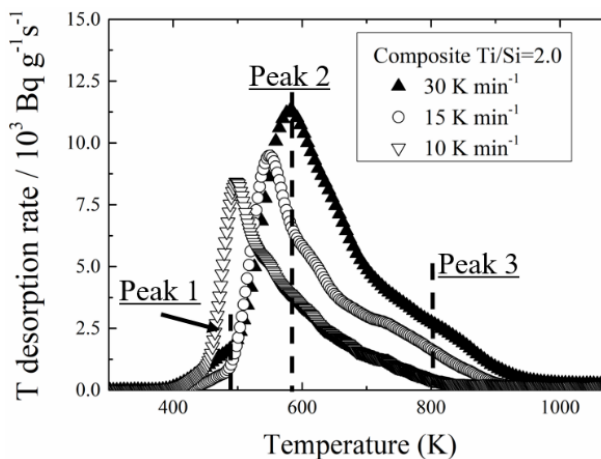

Fig. 2. Tritium-TDS spectra of composite Ti/Si=2.0 at different heating rates.

REFERENCES:
[1] Q. Zhou, *et al.*, J. Eur. Ceram. Soc., **34** (2014)801-807.
[2] M. Kobayashi, *et al.*, Fusion Eng. Des., **87**(2012) 475.

Sub-THz Absorption Bands of Ionic Liquids

T. Awano and T. Takahashi[1]

Faculty of Engineering, Tohoku Gakuin University
[1]Research Reactor Institute, Kyoto University

INTRODUCTION: We have observed millimeter wave absorption bands of silver or cuprous iodides superionic conductive glasses in sub-terahertz region[1]. These bands are due to conducting ions because there frequency difference is coincident with the square root of the ratio of their atomic masses. On the other hand, these bands seem to be due to collective motion of the conductive ions because their frequencies are lower than those estimated from their ionic masses. However, the dynamics of the collective movement of ions is not clear yet.

Ionic liquids(ILs) are molten salts even at room temperature. It is interesting to compare ionic motion in ILs with those in superionic conducting glasses to making clarify influence of glass network upon the collective motion of ions.

Recently, we have found sub-terahertz absorption bands of ILs[2]. These bands disappear at low temperatures at which the IL is solid. Therefore, these bands are due to ionic movement. However, the thermal change of absorption spectra of these ILs were various. This difference seems to be due to the difference of the process of their phase transition to the solid states (crystal or glass).

In this study we have measured millimeter wave absorption spectra of 33 ILs to make clear the ionic movement from the temperature change of absorption spectra.

EXPERIMENTS: A fixed amount of ionic liquids (Tokyo Chemical Industry Co., Ltd.) were spread into filter paper. Transmission spectra of single and double papers with ionic liquids were measured at room temperature and low temperatures. Absorption spectra were obtained by subtraction of them. To confirmation, measurements were repeated twice or three times for each IL. Molecular dynamics simulation was executed using Gromacs 5.0.

RESULTS: Four types of the spectral change occurred at temperature above melting point or glass transition temperature. The intensities of the absorption bands in the ILs which are crystal in solid state showed rapid decrease at their melting points. On the other hand, those in ILs which are vitreous in solid state weakened and shifted gradually. Some others showed complicated change. The other type showed no absorption in this spectral range. Figures 1(a) - (d) show typical spectra of these four types. Figure 2(a) shows rotational velocity autocorrelation function of cation and anion in [C$_2$min][Tf$_2$N], and figure 2(b) shows temperature dependence of that of the anion obtained by the MD simulation. Observed sub-THz bands seems to be due to rotational motion of the ions
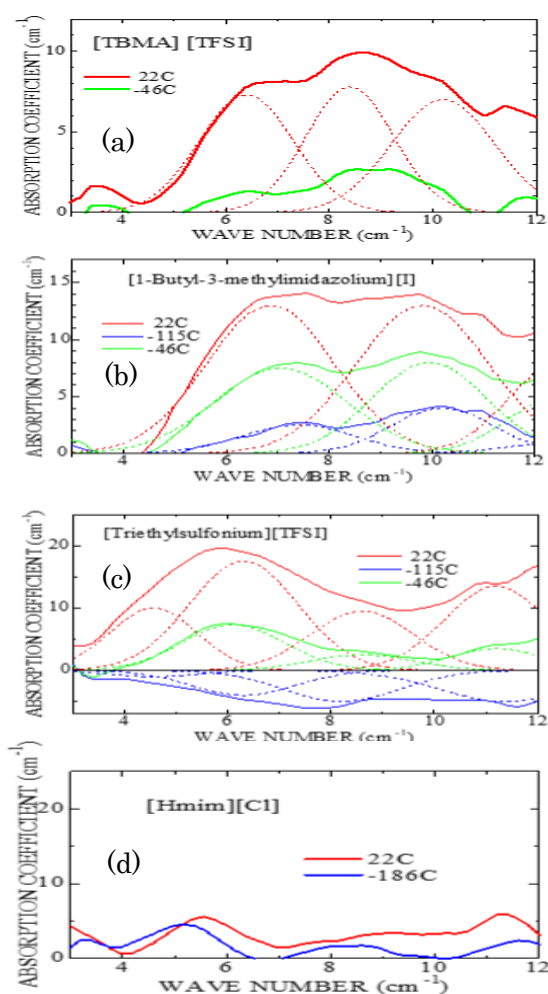

Fig. 1. Typical temperature dependence of absorption increment spectra of ionic liquids. The baseline is the absorption spectrum at 88 K.
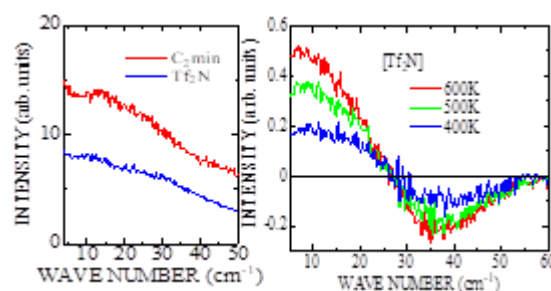

Fig. 2.(a) Rotational velocity autocorrelation function of the cation and anion at 300 K. (b) Increment spectra of anion against that at 300 K.

REFERENCES:
[1] T. Awano and T. Takahashi, J. Phys. Soc. Jpn. **79** Suppl. A (2010) 118-121.
[2] T. Awano , A. Shikoda and T. Takahashi, 21th International Conference on Solid State Ionics, (2017) IV-6 P.

CO4-8   The Correlation between Microstructural Evolution and Mechanical Property Changes in Neutron-irradiated Vanadium Alloys

K. Fukumoto, T. Onitsuka, Y. Tabata[1] and Xu Qiu[2]

RINE, Univ. of Fukui
[1]Graduate school of Eng., Univ. of Fukui
[2]KUR, Kyoto Univ.

INTRODUCTION: Vanadium alloys are candidate materials for fusion reactor blanket structural materials, but the knowledge about the mechanical properties at high temperatures during neutron irradiation is limited and there are uncertainties that may have influenced the results such as the interstitial impurity content of specimens. Recently, material irradiation technology in a liquid metal environment was developed and irradiation experiments in various liquid metal environments can be performed for vanadium alloys. Environmental effects and irradiation effects for mechanical properties should be distinguished independently in order to understand the essential behavior of vanadium alloys during irradiation for fusion reactor application. The objective of this study is to investigate the mechanical properties and microstructural changes of the vanadium alloys, V-4Cr-4Ti alloys during neutron irradiation. In this study, tensile test was carried out for V-4Cr-4Ti and V-4Cr-4Nb alloys to investigate the effect of Ti addition in ternary alloy of V-Cr system.

EXPERIMENTS: The majority of test specimens for this study were prepared from V-4Cr-4Ti, V-3Fe-4Ti and V-4Cr-4Nb alloys. The tensile specimens had nominal gauge dimensions of 0.25mm(t) x 1.2mm(w) x 5mm(l). Before irradiation, all specimens were annealed in vacuum at 1000°C for 2hrs. The specimens were irradiated in Joyo in the temperature range from 450°C to 650 °C with total neutron dose from 0.47 to 2.1 x 10^{26} n/m^2. In the previous study, the ratio of damage level, displacement per atom (dpa) to neutron dose in pure vanadium in Joyo MK-II was 2.5 x 10^{-26} dpa/Φtot. The amounts of estimated damage level ranged from 1.2 to 5.3 dpa. Tensile tests were conducted at room temperature and 400°C with various strain rate ranged from 6.7x10^{-4} to 10^{-2} to obtain the information of strain rate sensitivity at high temperature. SEM observation for fractography after tensile test was carried out in KUR, Kyoto University.

RESULTS: Tensile tests for V-4Cr-4Ti , V-3Fe-4Ti and V-4Cr-4Nb alloys were carried out at 400 ºC at strain rates between 6.7x10^{-4} and 6.7x10^{-1}/s. The strain-rate dependence was determined for the lower yield stress σ_{LYS}. From the general relationship between flow stress and strain rate, the strain rate sensitivity (SRS) parameter is defined as follows[1];

$$m = \frac{1}{\sigma}\frac{d\sigma}{d\ln\dot{\varepsilon}} \qquad (1)$$

When the flow stress σ rises with the increase of strain rate $\dot{\varepsilon}$, i.e., m>0, slip deformation is a thermally activated process. When m<0, a barrier strength of obstacle against dislocation slip motion is weakened and leads to reduction of the flow stress, because increasing the strain rate decreases time available for solute diffusion to dislocations. Values of the SRS for the lower yield stress were determined for each irradiation condition and test temperature from a logarithmic fit to the lower yield strength data. Figure 1 shows the stress-strain curves for the irradiated V-4Cr-4Ti, V-4Cr-4Nb and V-3Fe-4Ti in this study. The data of SS-curves for three type alloys were so almost the same that V-3Fe-4Ti and V-4Cr-4Nb alloys had the larger irradiation hardening than V-4Cr-4Ti alloy. It indicates that the effect of Nb addition contributes to the larger irradiation hardening than that of Ti addition for V-Cr system. The value SRS of both V-4Cr-4Ti and V-4Cr-4Nb did not change so much that the contribution to impurity interaction for Ti atom and Ni atom might be the same.
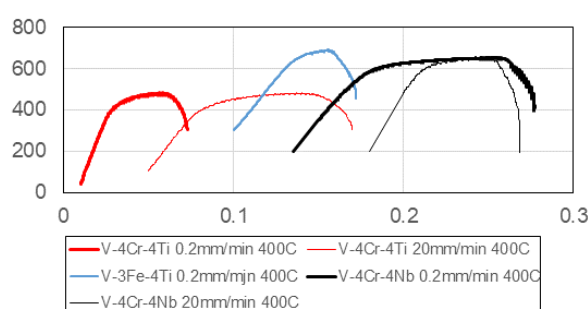

Figure 1 : The strain rate sensitivity (SRS) of lower yield stress dependence on the test temperature for the irradiated V-4Cr-4Ti alloy in this study and the previous data for V-4Cr-4Ti irradiated in HFBR [1].

Reference
[1] A. F. Rowcliffe, S. J. Zinkle and D. T. Hoelzer. J. Nucl. Mater., 283-287 (2000) 508-512

CO4-9   Defects Structure of Electron Irradiated B2 Ordered Alloys

F. Hori, Y. Sumikura, A. Takano, K. Kanazawa, A. Iwase, K. Ohsawa[1], Q. Xu[2] and N. Abe[2]

Dept. of Quantum & Radiation Eng., Osaka Pref. Univ.
[1]*Res. Inst. of Appl. Mech., Kyushu University*
[2]*Res. Reactor Inst., Kyoto University*

INTRODUCTION: We have been investigated radiation damage induced defects in intermetallic compound alloys, especially for B2 ordered Fe-Al alloys. Intermetallic compounds have good properties such as specific strength to weight ratio, oxidation resistance and strength in elevated temperature. However, the nature of basic defects in intermetallic compound alloys is not necessarily cleared yet. The reason why intermetallic compound alloys possibly include more than two types of vacancies, that is A-vacancy and B-vacancy in A-B compound alloy. It is difficult to distinguish these vacancies in any other experimental methods except for positron annihilation techniques. However, the amount of defect and the defect structure affects the various characteristic features, such as strength and electronic conductivity and so on. On the other hand, we have reported that vacancies introduced by electron irradiation strongly depend on incident electron energy because of their different threshold energy of displacement for each elemental atom. In Fe-Al alloys, we have shown that different energy of electron irradiation successfully produces different type of vacancy in Fe-Al alloys. In this study, we have tried to control the vacancy type induced by different energy of electron in another B2 ordered alloy system of Fe-Rh.

EXPERIMENTS: Fe-50%Rh alloy specimens with B2 structure were prepared by arc melting method. Sliced samples with the thickness of 0.5 mm were annealed at 1073 K for 3 h followed by quenched into water. These specimens were irradiated with 2 MeV electron to the fluence of 1×10^{17} and 1×10^{18} /cm^2 at JAEA-Takasaki and with 8 MeV electron to the fluence of 5×10^{17} and 1×10^{18} /cm^2 at KURRI, Kyoto University. In both cases, irradiations were carried out at about 330 K controlled by water flow system. After and before irradiation, samples were examined by X-ray diffraction, positron annihilation lifetime and coincidence Doppler broadening measurements. The positron lifetime spectra were analyzed by using POSITRONFIT program.

RESULTS: As shown in Table 1, positron lifetime before irradiation was not single component, which has longer lifetime component. This fact reveals that thermally vacancy was not annealed out perfectly in this sample. Essentially, it is well known that vacancy type defects in Fe-Al alloy is hardly to remove even in stoichiometry. After 1×10^{18} /cm^2 electron irradiation, positron lifetime increases in both irradiation cases. However, it appears slight larger positron lifetime for 8 MeV irradiated sample than that for 2 MeV irradiation case. This difference may be caused by twice larger displacement cross section for Rh than that for Fe above 4 MeV electron irradiation (Fig.1).

Table 1 Positron lifetime in each sample.

	τ1 (ps)	τ2 (ps)
unirrad.	121	173
2MeV	122	181
8MeV	145	186
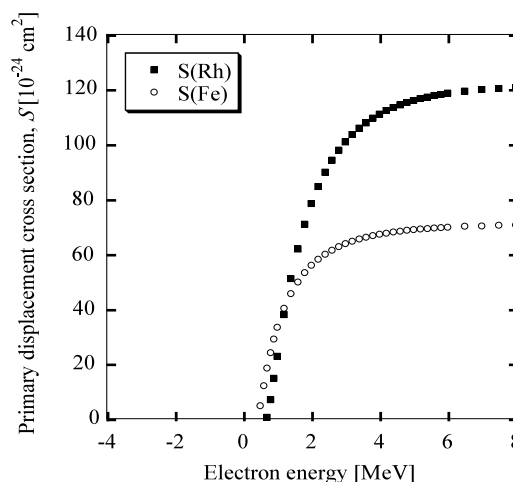
Fig. 1 Primary displacement cross section as a function of enectron energy.

29039

CO4-10   Synthesis of Multi-component Metal Nanoparticles by γ-ray Irradiation Reduction Method

F.Hori, M.Tanaka, S.Toda, M.Tani, A.Iwase, K.Okitsu[1], T.Matsui[2], Y.Mizukoshi[3] and Q.Xu[4]

Dept. of Engineering, Osaka Prefecture University
[1]*Dept. of Sustainable System Science, Osaka Prefecture University*
[2]*Center for Advanced Education of Entrepreneurship and Innovation, Osaka Prefecture University*
[3]*Institute of Materials Research, Tohoku University*
[4]*Research Reactor Institute, Kyoto University*

INTRODUCTION: It is well known that metal nanoparticles (NPs) have some specific properties, which are not appeared in bulk materials such as catalytic activities, magnetic properties, electric conductivity and light absorption. These properties depend on its size, shape, structure, chemical composition and so on. They have many possibilities to applied for various industrial fields. However, it is not easy to fabricate multi elemental alloy NPs with controlling their size, shape and structure. Generally, many kinds of metal NPs commercially are synthesized by using chemical reaction method, which is not necessarily in water solution. Recent years, some reports show that it is possible to fabricate some metal NPs under irradiation reduction fields such as ultrasonic, solution plasma, electron beam, ion beam and gamma-ray [1]. We have been trying to synthesize various kinds of metal nanoparticles with size and shape controlled by gamma-ray irradiation reduction method. In this study, we have tried to synthesize pure Cu and Cu-Au multi component alloy NPs by gamma-ray irradiation.

EXPERIMENTS: Aqueous solution with a given concentration of copper complex $((CH_3COO)_2Cu \cdot H_2O)$ with an additive of sodium dodecyl sulfate (SDS) and 8.5 vol% ethylene glycol. The solution was argon gas purged and sealed into polystyrene vessels. They were irradiated at about 300 K with 1.17 and 1.33 MeV gamma-rays from ^{60}Co radio active source at gamma irradiation facility in KURRI, Kyoto University. The total dose was fixed to 10 kGy with the dose rate of 2.0 kGy/h. After first irradiation, 1.0 mM gold complex $(NaAuCl_4 \cdot 2H_2O)$ was added and irradiated it with 10 kGy continuously. The shapes and the structures for all colloidal products were observed by TEM (JEM-2000FX and FEI-Titan) and energy dispersive X-ray spectrometry (EDS). Samples for TEM observations were made by putting a drop of colloidal solutions on a carbon film with a Mo mesh and dried them in a vacuum. X-ray Photoelectron Spectroscopy (XPS) measurement at KEK-PF BL-27 has performed.

RESULTS:
Fig. 1 shows the TEM-EDS images for NPs formed in aqueous solutions after two second gamma-ray irradiation. This figure shows that Au-core and Cu-shell NPs are formed by this irradiation process. XPS result also shows existing of pure Cu metal in this NPs and it remains stable after 4 month (Fig. 2). On the other hand, UV-vis absorbance spectra shows only one absorption peak around 520 nm, which shows Au surface plasmon resonance. From these results, it can be concluded that Au-NPs covered with extreme thin Cu layers (at least one or two layers) were formed so that surface plasmon resonance of Au arises.
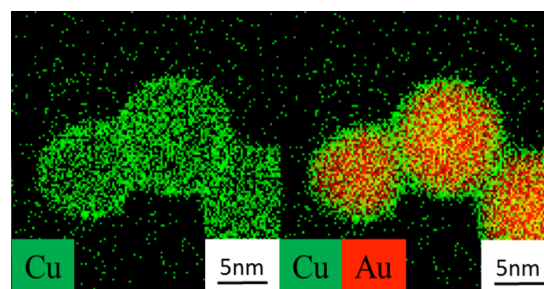

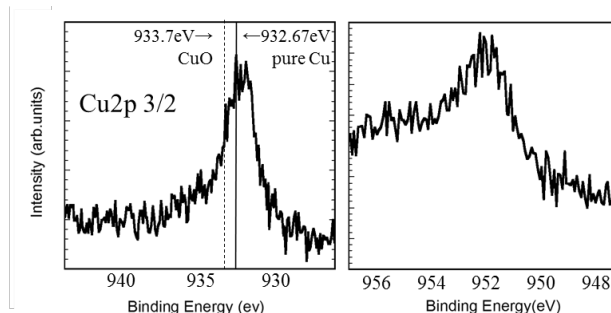Fig.1 EDS images of synthesized nanoparticles after two steps gamma-ray irradiation reduction.

Fig. 2 XPS spectra of NPs exposed to air after two months.

References
[1] N.Taguchi and F.Hori *et al.*, Rad. Phys. Chem., **78** (2009) 1049-1053.

Radioactivation of Accident Tolerant Control Rod Materials

H. Ohta, Y. Nauchi, K. Nakamura and T. Sano[1]

Nuclear Research Technology Laboratory,
Central Research Institute of Electric Power Industry

[1]*Institute for Integrated Radiation and Nuclear Science,*
Kyoto University

INTRODUCTION: As an effort to improve the safety of light water reactors (LWRs), various concepts of "enhanced accident tolerant fuels and core components" are being developed in many countries. The Central Research Institute of Electric Power Industry (CRIEPI) has been developing an accident tolerant control rod (ATCR) to which the novel neutron absorbing materials including rare-earth sesquioxides (RE_2O_3) are applied [1]. The ATCR improves the basic performance as a control rod such as the reactor shutdown margin and neutronic lifetime, and reduces the risk of re-criticality accident in any reactor conditions including severe accident (SA). For the ATCR candidate materials RE_2O_3-MO_2 (RE = Sm or Eu, M = Zr or Hf), a high temperature compatibility with iron or steel, which is a main component of current control rod cladding, and physicochemical stability under high temperature steam atmosphere were experimentally confirmed so far [2]. Furthermore, a reactivity analysis in representative LWRs revealed that these candidate materials have enough reactivity worth comparable to or higher than the conventional neutron absorbing materials B_4C or Ag-In-Cd alloy [1]. Since the control rods are arranged inside or very close to the operating core for a long period, the irradiation characteristics of the candidate materials are needed to be confirmed. In this study, the radioactivation characteristics of Sm_2O_3, Eu_2O_3 and ZrO_2, which are irradiated for short terms are measured toward the future long-term irradiation tests.

EXPERIMENTS: Irradiation experiment conditions are summarized in Table I. The powder of each material was packed in Al container with 8mm in diameter and 9.5mm in depth. The strong neutron absorbing materials, Sm_2O_3 and Eu_2O_3 were diluted with the powder of a neutronic inert material Al_2O_3 to reduce the self-shielding effect. For a preparation of ZrO_2 sample, highly pure Zr with impurity Hf of ~0.0055wt% were used. Irradiation experiments were performed for 10 minutes or 4 hours using a pneumatic tube No.2 (Pn-2) in KUR operating at rated power 1MW. Then, gamma-ray emitted from each sample irradiated for 10 minutes were measured with an HP-Ge detector, and the induced radioactivities were evaluated. The samples irradiated for 4 hours are still cooled.

The detection efficiency of the HP-Ge detector applied in this study was calibrated with a multi-isotope mixed standard gamma-ray source in the range of 60keV to 1836keV, and the obtained curve is shown in Fig. 1.

Table I. Irradiation Experiment Conditions

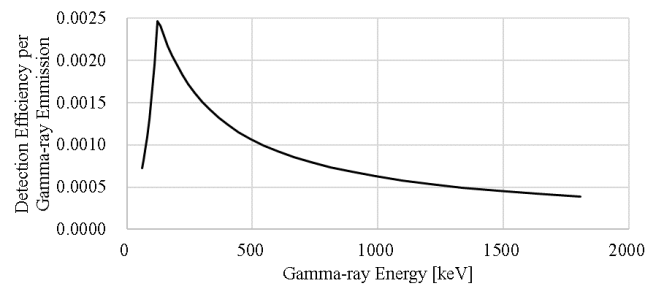|	Sm_2O_3	Eu_2O_3	ZrO_2
Sample Specifications			
Container diameter	8mm	←	←
Container Height	9.5mm	←	←
Weight	2.38mg	0.425mg	1.105g
Diluent	Al_2O_3	←	-
Irradiation			
Position	Pn-2	←	←
Period	10min./4hr.	←	10min.

Fig. 1. Detection efficiency curve of HP-Ge detector.

RESULTS: For representative neutron absorption reactions of Sm, Eu and Zr as shown in following (1) - (5), gamma-ray intensities from the neutron absorption products were measured and the radioactivities of these samples at the end-of-irradiation were evaluated.
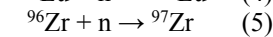
$$^{152}Sm + n \rightarrow {}^{153}Sm \quad (1)$$
$$^{151}Eu + n \rightarrow {}^{152m}Eu \quad (2)$$
$$^{151}Eu + n \rightarrow {}^{152}Eu \quad (3)$$
$$^{153}Eu + n \rightarrow {}^{154}Eu \quad (4)$$
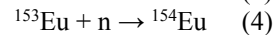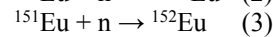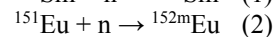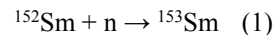$$^{96}Zr + n \rightarrow {}^{97}Zr \quad (5)$$

Table II summarizes the results of radioactivities evaluated from gamma-ray measurement, compared with predictions based on neutron absorption cross-sections for 0.025eV and thermal neutron flux in Pn-2 (5.50E+12 n/cm^2·s). These results indicate that the radioactivation characteristics of Sm_2O_3, Eu_2O_3 and ZrO_2 irradiated for 10 minutes are analytically predictable. Subsequently, the radioactivities of the other samples irradiated for 4 hours are also evaluated and longer-term irradiation test conditions will be discussed.

Table II Radioactivity of Sm_2O_3, Eu_2O_3 and ZrO_2 irradiated for 10minutes

Sample isotope	Produced isotope	Half life	Radioactivity [Bq/gram-sample]	
			Measurement	Prediction
^{152}Sm	^{153}Sm	46.3 hr.	3.263E+9	2.577E+9
^{151}Eu	^{152m}Eu	9.3 hr.	2.458E+11	3.529E+11
^{151}Eu	^{152}Eu	13.3 yr.	3.727E+7	5.365E+7
^{153}Eu	^{154}Eu	8.8 yr.	4.646E+6	5.412E+6
^{96}Zr	^{97}Zr	16.8 hr.	7.951E+5	9.774E+5

REFERENCES:
[1] H. Ohta, *et al.*, TopFuel 2016 (2016) 17556 .
[2] K. Nakamura, *et al.*, AESJ 2017 spring meeting. 1I06 in Japanese.

CO4-12   Neutron Irradiation Effect of High-density MoO$_3$ Pellets for Mo-99 Production

Y. Suzuki, K. Nishikata, Y. Namekawa, A. Kimura,
A. Shibata, N. Nakamura, K. Tsuchiya,
T. Sano[1], Y. Fujihara[1], and J. Zhang[1]

Department of JMTR, Japan Atomic Energy Agency
[1]Research Reactor Institute, Kyoto University

INTRODUCTION: The research and development (R&D) has been carried out for the production of Molybdenum-99 (^{99}Mo) by the neutron activation method ((n, γ) method) from viewpoints of limited availability of high-enriched uranium, no-proliferation and nuclear security, and disposal of nuclear fissile materials.   It is essential to improve the properties of Alumina (Al$_2$O$_3$) used widely as the ^{99}Mo/^{99m}Tc generator.   In this study, two kinds of Al$_2$O$_3$ specimens were prepared, and molybdenum adsorption and technetium-99m (^{99m}Tc) desorption properties of these Al$_2$O$_3$ specimens were evaluated.

EXPERIMENTS: The MoO$_3$ pellets were fabricated by the cold pressing and sintering Method.   Density of MoO$_3$ pellets was about 60%T.D.   The MoO$_3$ pellet pieces (about 1.5 g) were irradiated in the Pn-2 of the KUR.   Table 1 shows the irradiation conditions of MoO$_3$ pellets in the Pn-2.   After the irradiation tests, the irradiated MoO$_3$ pellet pieces were dissolved with 6M-NaOH solution.   Then, the Mo adsorption tests of the Al$_2$O$_3$ specimens were carried out with the sodium molybdate solution (10mg-Mo/mL at pH4) at RT.   After the tests, each Al$_2$O$_3$ specimen adsorbing Mo was packed in the polypropylene column.   The saline was flowed through in this column and the ^{99m}Tc was extracted from each Al$_2$O$_3$ specimen. In this test, the activities of ^{99}Mo and ^{99m}Tc in the solution were measured by the Gamma-ray spectrometer.

Table 1 Irradiation conditions of MoO$_3$ pellet pieces in Pn-2.

Items	Values
Thermal power	5 MW
Thermal neutron flux	2.8×10^{17} m^{-2}s^{-1}
Epithermal neutron flux	1.1×10^{16} m^{-2}s^{-1}
Fast neutron flux	6.0×10^{16} m^{-2}s^{-1}
Irradiation time	20 min.

RESULTS: Table 2 shows the activities of ^{99}Mo and ^{99m}Tc in the sodium molybdate solution after about 100 h from irradiation completion.   The calculation value was evaluated by thermal neutron flux and correction by half time.   In this experiment, the ratio of ^{99m}Tc and ^{99}Mo was about 0.95 except for the result of Run 1 and the ratio was almost the same as the ratio of calculation value. On the other hand, the ratios of calculation value and experimental value (C/E) of ^{99}Mo and ^{99m}Tc were about 0.456 and 0.448, respectively.   In order to evaluate

^{99}Mo generation, it is necessary to take into account the ^{98}Mo absorption rate in epi-thermal and fast region. [1].

Table 2 Activities of ^{99}Mo and ^{99m}Tc in the sodium molybdate solution after about 100 h from irradiation completion.

| | Run 1 | | Run 2 | | | |
| | | | Specimen-1 (V-B-300) | | Specimen-2 (Medical) | |
	^{99}Mo	^{99m}Tc	^{99}Mo	^{99m}Tc	^{99}Mo	^{99m}Tc
Calculation values[*1] (MBq/g-MoO$_3$)	4.49	4.35	4.49	4.35	4.49	4.35
Experimental values[*2] (MBq/g-MoO$_3$)	9.79	10.4	9.92	9.27	9.80	9.54

*1 : Calculation values by thermal neutron flux and correction by half time.
*2 : Measurement values by the γ-ray spectrometer.

Table 3 shows the result of ^{99}Mo adsorption amounts of Al$_2$O$_3$ specimens and ^{99m}Tc recovery rates from Al$_2$O$_3$ specimens.   The Mo adsorption amounts of V-B-300 and medical Al$_2$O$_3$ were 83.1 and 24.3 mg-Mo/g-Al$_2$O$_3$, respectively.   These values were almost the same as the values with un-irradiated Mo solution.   It seems that the Mo adsorption properties were influenced to crystal structure and specific surface of Al$_2$O$_3$ specimens [2].   In the result of milking process, the ^{99m}Tc recovery property of V-B-300 was better than that of the medical Al$_2$O$_3$. On the other hand, the ^{99m}Tc recovery property was decreased for each milking.

Table 3 Results of ^{99}Mo adsorption amounts of Al$_2$O$_3$ specimens and ^{99m}Tc recovery rates from Al$_2$O$_3$ specimens

Items	Specimen-1 (V-B-300)	Specimen-2 (Medical)
^{99}Mo adsorption amounts (Bq/g-Al$_2$O$_3$) (mg-Mo/g-Al$_2$O$_3$)	1.32×10^6 83.1	3.86×10^5 24.3
^{99m}Tc recovery rates in Milking 1st run 2nd run 3rd run	93.5 % 87.6 % 84.5 %	74.1 % 61.6 % 54.8 %

CONCLUSION: The MoO$_3$ pellets were irradiated in the Pn-2 at KUR, and ^{99}Mo adsorption/^{99m}Tc recovery properties of the Al$_2$O$_3$ specimens were evaluated with the solution of the irradiated MoO$_3$ pellets. The Mo adsorption amounts of V-B-300 and medical Al$_2$O$_3$ were almost the same as the values with un-irradiated Mo solution.   In future, it is necessary to perform the detail evaluation of neutron flux in Pn-2 and ^{99}Mo adsorption/^{99m}Tc recovery properties of various Al$_2$O$_3$ specimens.

REFERENCES:
[1] K. Nishikata, *et al*., CO4-21, KURRI Progress Report 2013, (2013), P.242 .
[2] Y. Suzuki, *et al*., Transactions of the Materials Research Society of Japan, **43**(2018)73-80.

CO4-13 Reserch on Resonance Frequency Variation as Function of Exposure Radiation Dose

M. Kobayashi, T. Miyachi, S. Takechi[1], S. Fujita[1] and N. Konishi[1]

Planetary Exploration Research Center, Chiba Institute of Technology
[1]Graduate School of Engineering, Osaka City University

INTRODUCTION: In the previous studies, we have performed experiments that a piezoelectric element was irradiated with high intensity 400 MeV/n Xe beam at HIMAC of the National Institute of Radiological Sciences [1][2]. As a result, we found that when irradiating a very strong radiation to a piezoelectric element, its resonance frequency and anti-resonance frequency are shifted and also the impedance at the resonance frequency and anti-resonance frequency are changed by beam irradiation. In particular, it was found that the resonance frequency increases linearly with the irradiation amount.

Since the piezoelectric element is a crystalline material, it is considered that the crystal is damaged by the beam irradiation, and thus the characteristic parameter such as the resonance frequency has changed. Although it is considered to be some radiation damage, detailed mechanism such as its mechanism is not known. Radiation damage roughly includes damage due to ionization and non-ionization, but since ionized Xe beam has both ionization and non-ionizing effects, it is difficult to determine which effect mainly affects the piezoelectricity.

Therefore, in this study, we investigated the response of the piezoelectric parameter to energetic electron beam which has dominantly ionizing effect (less non-ionizing effect).

EXPERIMENTS: A piezoelectric element was placed in the beam line by KURRI-LINAC as an electron beam source. Before obtaining experimental data, we performed preliminary runs to find appropriate test set up and electron beam condition. The test piece of PZT element can be warmed by electron beam irradiation due to high intensity, the piece was air-cooled by a fan to keep the temperature lower than 100 ℃ otherwise the piezoelectricity can be quickly vanished due to high temperature. We monitored the temperature of the test piece and adjusted the beam current as beam intensity to be around 0.8 ~ 1.0 μA not to heat it higher than 100 ℃.

After fixing the test setup and beam condition, we had four runs to obtain experimental data.

RESULTS: Fig. 1 and Fig. 2 show changes of resonance frequency and anti-resonance frequency during electron beam irradiation with a constant beam current of 1.0 μA. At 0 to 10 min of the elapse time, those frequencies changed rapidly because the PZT element temperature was changed by beam irradiation and then became stable after temperature achieved equilibrium. Even in stable temperature, those frequencies were slightly increased. Fig.3 shows only plots in thermal equilibrium period. The frequency was linearly increased with time, namely irradiation dose. That is the same trend as Xe

beam experiment. Xe beam experiments, however, did not show increase in anti-resonance frequency as this study. We will investigate quantitatively the experiment results in further analysis to compare with Xe beam results.
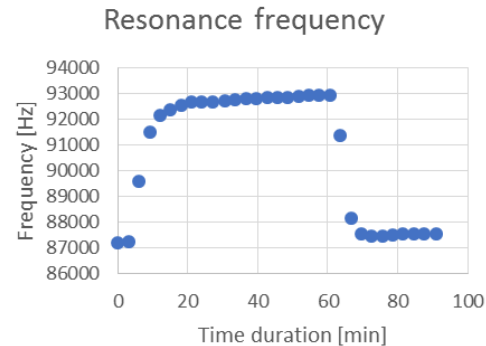

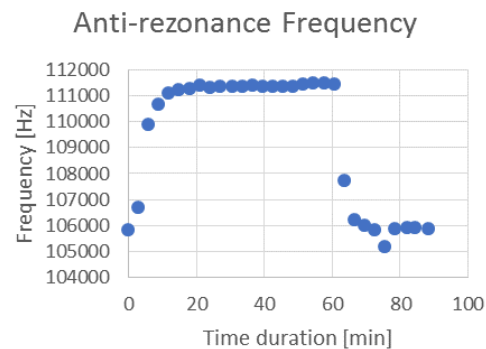Fig.1 Resonance frequency change during electron beam irradiation with 1.0 μA.

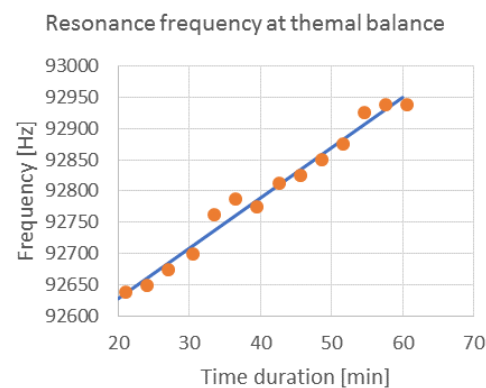Fig.2 Anti-resonance frequency change during electron beam irradiation with 1.0 μA.

Fig. 3 Plots of frequency as function of time ranging 20 min to 60 min of Fig.1.

REFERENCES:
[1] M. Kobayashi *et al.*, Japanese Journal of Applied Physics, **53** (2014) 066602 .
[2] M. Kobayashi *et al.,* Japanese Journal of Applied Physics, **52** (2013) 126604.

CO4-14   Selection of Borosilicate Glass Composition for Neutron Irradiation Test

T. Nagai, A. Uehara[1] and T. Fujii[2]

Japan Atomic Energy Agency (JAEA)
[1]Research Reactor Institute, Kyoto University
[2]Graduate School of Engineering, Osaka University

INTRODUCTION: A high-level radioactive liquid waste from a reprocessing process for spent nuclear fuels is processed into a solidified waste glass made by using a borosilicate glass as media. In our previous study [1], the neutron irradiation test of a borosilicate glass sample $19Na_2O-17B_2O_3-63SiO_2-CeO_2-Y_2O_3$ was carried out under the condition of 1000 kW for 10 min in KUR in 2014FY, and the structural change after the irradiation was observed slightly by using Raman spectrometry.

In this study, to understand the structural change of a borosilicate glass by a neutron irradiation in detail, the neutron irradiation test was carried out for 50 min in the Pn-2. The structural change of glass sample after the irradiation will be estimated in 2018FY. This is the intermediate report.

EXPERIMENTS: Before the irradiation test, the glass composition was selected to estimate a structural change accurately. As a result of the previous study [1], we thought that Li content in the sample would be increased by the $^{10}B(n,\alpha)^7Li$ reaction, and a connection of the Si-O bridging structure might be cut by the generated Li. To confirm the change of Raman spectrum by adding Li, $8Li_2O-11Na_2O-17B_2O_3-64SiO_2$ and $19Na_2O-17B_2O_3-63SiO_2$ were prepared, and their spectra were measured. As shown in Fig. 1, measured spectrum of $8Li_2O-11Na_2O-17B_2O_3-64SiO_2$ has a higher intensity around $1000cm^{-1}$ than the other. Therefore, it would be easy to estimate the structural change by applying a Li free borosilicate glass in this irradiation test.

With a consideration above-mentioned, two kinds of borosilicate glass, $17Na_2O-17B_2O_3-65SiO_2-CeO_2-Y_2O_3$ and $17Na_2O-28B_2O_3-54SiO_2-CeO_2-Y_2O_3$ were selected. The raw material reagents of SiO_2, H_3BO_3, Na_2CO_3, CeO_2, and Y_2O_3 were placed in an alumina crucible and were melted at 1150°C in an electric furnace. After the molten glass samples were solidified by cooling to room temperature, they were cut into thin plates.

In Dec. of 2017, the glass samples of thin plate were set in a polyethylene tube and were irradiated under the condition of 1000 kW for 50 min in the Pn-2 of KUR.

After the radioactivity of the samples is sufficiently attenuated, the Raman spectra of the glass sample will be measured by using a laser Raman spectrometer, NRS-3100 of JASCO in KUR in 2018FY.

RESULTS: On the selection of glass composition for the neutron irradiation test, Raman spectra of $8Li_2O-11Na_2O-17B_2O_3-64SiO_2$ and $19Na_2O-17B_2O_3-63SiO_2$ were measured by using a laser Raman spectrometer,

NRS-5100 of JASCO in JAEA as shown in Fig. 1.

The Raman spectrum of Si-O bridging structure of a silicate glass were in the wavenumber of 850-1200 cm^{-1}, and the peak positions of Raman shifts were different from the number of non-bridging oxygen, NBO, of the Si-O structure [2]. In this measurement of borosilicate glass, those Raman shifts were observed in 850-1250 cm^{-1} and the measured spectra could be separated into Gaussian waves as shown in Fig. 1. The Raman peak of Q^4 structure without NBO appeared in 1140-1150 cm^{-1}, and those of Q^3, Q^2, and Q^1 structures with the NBO number = 1, 2, and 3 were in 1070-1090, 1000-1020, and 920-930 cm^{-1} respectively. The peaks of Q^2 and Q^3 can be subdivided into plural by the Si-O-X connecting state, and only Q^3 in Fig. 1 was divided into 2 peaks of $Q^{3(1)}$ and $Q^{3(2)}$. When the change of Raman spectrum by adding Li, it can be observed that the peak heights of Q^4, $Q^{3(1)}$ and $Q^{3(2)}$ decreased and those of Q^2 and Q^1 increased. These changes by a adding Li was similar to that by the neutron irradiation for 10 min in previous study [1].

This neutron irradiation effect can be confirmed clearly by measuring a Raman spectrum of the glass sample irradiated for 50 min.
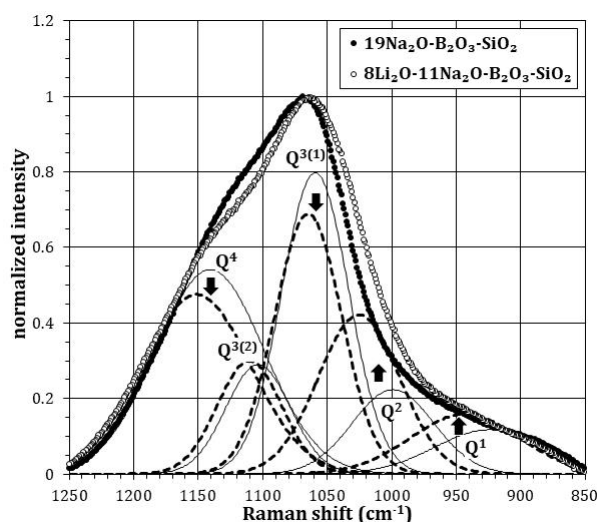

Fig. 1. Raman spectra of $8Li_2O-11Na_2O-17B_2O_3-64SiO_2$ (open circle, dashed lines) and $19Na_2O-17B_2O_3-64SiO_2$ (closed circle, fine lines) for selecting glass composition of neutron irradiation test.

REFERENCES:
[1] T. Nagai, *et al*, 2009FY KURRI Progress Report, 2014 (2015) 26P11-4.
[2] P. McMillan, Am. Mineralogist, **69** (1984) 622-644.

CO4-15   **Formation of Nano-porous Structures on Whole Surface of Ge
Wafer by High-energy Ion Irradiation**

J. Yanagisawa, Q. Xu[1], A. Yabuuchi[1], K. Takamiya[1], and
A. Kinomura[1]

School of Engineering, The University of Shiga Prefecture
[1]*Research Reactor Institute, Kyoto University*

INTRODUCTION: We have been reported that the high-energy (100 keV) focused gallium (Ga) ion beam (Ga FIB)-irradiated area of germanium (Ge) wafer surface was changed to porous structures with nanometer size (nano-porous structures) [1]. It is also found that the size and the shape of such nano-porous structures can be controlled by the FIB irradiation conditions, such as dwell time, ion beam current and total fluence of the FIB. Because such nano-porous structures have large specific surface area, an improvement of the efficiency of surface-related phenomena, such as photocatalytic action, can be expected. However, the formation of such nano-porous structures on whole area of a chip of a Ge wafer surface using FIB is difficult because of the small spot size of the FIB. Therefore, we have tried to form such nano-porous structures on the whole area of the Ge sample surfaces using the large-area ion implantation apparatus in this laboratory. In this system, the ion species used was argon (Ar) and the operation energy was 60 keV, which were different from the previous studies using the Ga-FIB at 90 – 100 keV.

The aim of the present study is to confirm the formation of the nano-porous structures on a whole area of Ge (110) surfaces by 60 keV Ar ion irradiation.

EXPERIMENTS: About 1 cm x 1 cm chip samples were prepared from a Ge (110) wafer by cleavage. After cleaning of them using ultrasonic bath, a corner part of each sample was covered by aluminum foil to prevent the ion irradiation.

Ion irradiation was performed using Ar ions at an energy of 60 keV. Ion irradiated area was 1.51 x 1.55 cm^2. Three kind of samples were prepared using the different ion current and total fluence, that is 0.6 μA and 1 x 10^{16} cm^{-2} (sample 1), 5 μA and 5 x 10^{16} cm^{-2} (sample 2), and 13 μA and 1 x 10^{17} cm^{-2} (sample 3), respectively.

After the ion irradiation, the change of the sample surface was firstly observed by an optical microscope. Then the surface morphology and the atomic composition of the surface were measured using the energy dispersive x-ray spectroscopy – scanning electron microscope (EDS-SEM) system (PHENOM PROX).

RESULTS and DISCUSSION: Figure 1 shows the optical microscope image of the surface of the sample 3 with the Ar ion fluence of 1 x 10^{17} cm^{-2}. It is found that the ion-irradiated area was obviously changed to dark. The darkness was increased with increasing the total fluence of the Ar ions (the result is not shown in this report).
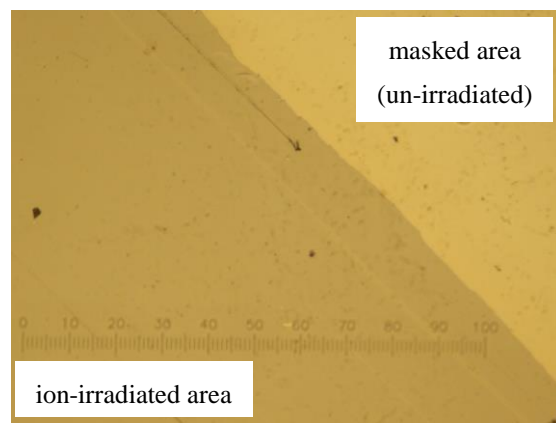

Fig. 1. Optical microscope image of ion-irradiated

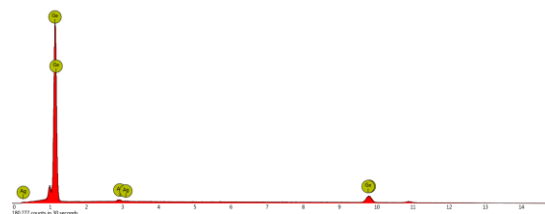and un-irradiated area of Ge wafer surface (x200).

Fig. 2. EDS spectrum from the ion-irradiated area
of the surface of sample 3.

One suspected reason for the darkness is the formation of a film of carbon-related materials, because of the temperature rise of the sample surface and/or other ion irradiated effects due to longer ion irradiation time and larger ion beam current (in case of sample 3, about 42 min. and 13 μA, respectively). To confirm this, the atomic concentration of the ion-irradiated area of the sample 3 was measured using the EDS-SEM. The result is shown in Fig. 2. The atomic concentration was Ge : Ag = 97.8 : 2.2, no carbon was detected. Although the origin of Ag is not clear at present, this result indicates that at least the observed darkness of the ion-irradiated area is not due to the carbon-related materials, but is due to the formation of sub-micron structures, which change the reflectance ratio of the visible light, by the 60 keV Ar ion irradiation. In fact, lurking small structures were observed during the EDS-SEM observation of the ion-irradiated area.

CONCLUSION: 60 keV Ar ion irradiation was performed on whole area of Ge (110) surfaces. Although high-resolution SEM observation is necessary, the present result indicates that the formation of, at least, sub-micron (or nano-) structures can be obtained by the present ion irradiation conditions.

REFERENCE:
[1] J. Yanagisawa, K. Takarabe, K. Ogushi, K. Gamo and
    Y. Akasaka, J. Phys.: Condens. Matter **19** (2007)
    445002 (10pp).

Development of ^{57}Co Mössbauer Source Using KURRI-LINAC

Y. Kobayashi, T. Kubota, M. Saito, R. Masuda, M. Ku-
rokuzu, S. Kitao and M. Seto

*Institute for Integrated Radiation and Nuclear Science,
Kyoto University*

INTRODUCTION: On Mössbauer emission spectroscopy, the activated sample containing the Mössbauer-parent nuclei is used as a γ-ray source. The intensity of the emitted Mössbauer γ-ray from the sample is measured after transmitting a standard absorber as a function of the relative velocity of the source (sample) and the reference absorber. This technique allows for Mössbauer studies of samples containing relatively low amount of the Mössbauer nuclei e.g., low concentration dopants, thin films, surface of materials.

The purpose of this study is to demonstrate the production of ^{57}Co whose amount is sufficient for the ^{57}Fe-Mössbauer measurement using KURRI-LINAC. Here, ^{57}Co (half-life: 270 d) is the γ-ray source of ^{57}Fe Mössbauer spectroscopy. On KURRI-LINAC, we can produce radio isotopes by photonuclear reaction using the bremsstrahlung X-ray, which is emitted from the noble-metal target. By photonuclear reaction, we can produce ^{57}Co as daughter of ^{57}Ni (half-life: 35.6 h), which is produced by ^{58}Ni(γ,n)^{57}Ni reaction. ^{57}Co is also produced by ^{58}Ni(γ,p)^{57}Co reaction, though the cross section of this reaction is lower than (γ,n) reaction.

EXPERIMENTS: On the irradiation of KURRI-LINAC, the energy of electron beam was 31 MeV, and the current was 190 μA. The target to generate the bremsstrahlung X-ray was water-cooled Pt metal, and the irradiation sample was put on the downstream side of the target. The sample was natural Ni metal foil (8 mg), and the irradiation time was 24 hours. Because the natural abundance of ^{58}Ni is relatively high (68%), natural Ni was used for the source.

For Mössbauer spectroscopy measurement, we used conventional Mössbauer spectrometer, and the irradiated sample was attached on the velocity transducer. The reference absorber was K$_2$MgFe(CN)$_6$, which shows a single peak spectrum on normal Mössbauer spectroscopy.

RESULTS: Figure 1 shows energy spectra of X-rays and γ-rays from the irradiated Ni. The γ-rays intensity from ^{57}Ni decreases with time; Instead, the γ-rays intensity from ^{57}Co increases as expected. Additionally, ^{61}Co (^{62}Ni(γ,p)^{61}Co, half-life: 1.65 h), ^{56}Ni (^{58}Ni(γ,2n)^{56}Ni, half-life: 6.1 d) and ^{56}Co (daughter of ^{58}Ni, half-life: 77 d) were observed as minor radio isotopes [1]; these were ignorable on Mössbauer measurement.

Figure 2 shows the obtained Mössbauer spectrum. It shows sextet reflecting magnetism of Ni metal. The hyperfine magnetic field evaluated by the fitting of the spectrum was 26.7 T, which is consistent with the reported value of ^{57}Fe in Ni metal [2]. This result shows that enough amount of ^{57}Co for the Mössbauer measurement can be produced using KURRI-LINAC and the Mössbauer emission spectroscopy is potentially available for application studies. In the future, we will perform ^{67}Zn-Mössbauer spectroscopy using the established methodology. Additionally, we attempt to extract ^{57}Co from irradiated Ni sample by the chemical operation and utilize it for e.g., a tracer experiment.
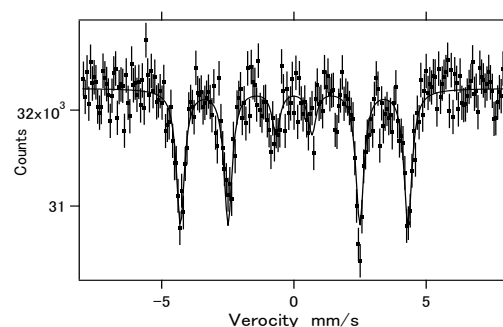

Fig. 2 Mössbauer spectrum obtained by using ^{57}Co source in Ni metal and K$_2$MgFe(CN)$_6$ absorber at room temperature.

REFERENCES:
[1] R. B. Firestone, in *Table of Isotopes*, 8th ed., edited by V. S. Shirley (Wiley, New York,1996), Vol. 1.
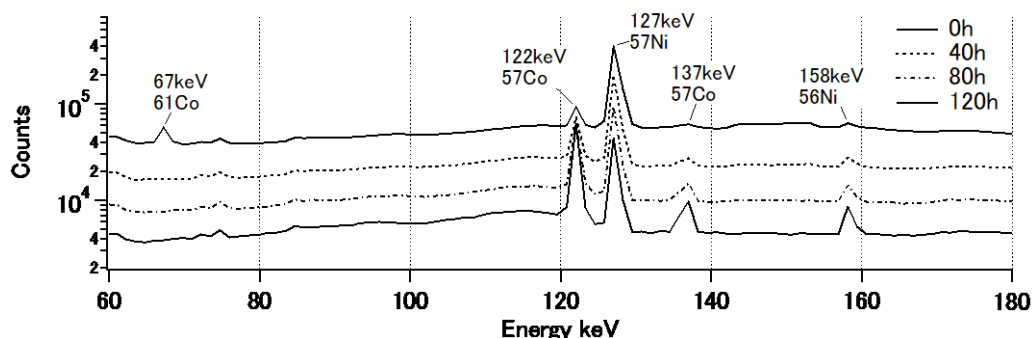[2] C. E. Johnson, M. S. Ridout and T. E. Cranshaw, Proc. Phys. Soc., **81** (1963) 107.

Fig. 1 Energy spectra of high-energy X-rays and γ-rays emitted from the Ni-foil source.

CO4-17   **Electrolytic Reduction of Calcium Oxide in CaCl$_2$-KCl Molten Salt Using Liquid Tin Cathode**

H. Sekimoto, Y. Haga[1] and A. Uehara[2]

Department of Physical Science and Materials Engineering, Faculty of Science and Engineering, Iwate University

[1]Department of Frontier Materials and Function Engineering, Graduate School of Engineering, Iwate University

[2]Research Reactor Institute, Kyoto University

INTRODUCTION: It is well known that it is difficult to produce metallic calcium by the electrolysis of CaCl$_2$ based molten salt at high current efficiency. Because metallic calcium deposited on chathode is easily re-oxidized on anode due to the high solubility of metallic calcium in CaCl$_2$ molten salt. And chlorine gas generated on anode also easily reacted with metallic calcium. Recently, Lukasko and Murphy developed an interesting technique that metallic calcium is once recovered as Sn-Ca alloy by the electrolysis of CaCl$_2$-KCl molten salt and then the Sn-Ca alloy is elctrorefined to pure metallic calcium at high current efficiency [1]. The feed of calcium in their technique is CaCl$_2$. This study is a progress of their process to change the feed to CaO. In this study, electrowinning of metallic calcium as calciujm-tin alloy from CaCl$_2$-KCl-CaO molten salt using liquid tin cathode was investigated.

EXPERIMENTS: All electrochemical experiments were carried out in an argon filled glove box, where the vapor pressure was controlled below 10 ppm. Metallic tin, CaCl$_2$, KCl, and CaO were weighed and put in an alumina crucible, which was then set in a vertical electric furnace. The sample was heated at 1000 K to prepare CaCl$_2$-65 mass%KCl molten containing 0 – 2.0 mass% of CaO and liquid tin. Then, tungsten wire inserted in an alumina tube was immersed in the metallic tin and a graphite rode inserted in a silica tube was immersed in the CaCl$_2$-KCl molten salt. Galvanostatic electrolysis using 2 electrodes of tin cathode and graphite anode was carried out at -0.4 A for 2 hours. After the electrolysis, W wire and graphite rod were removed and the sample was cooled to be solidified. The concentration of calcium in tin cathode was determined by ICP-OES to evaluate the cathode current efficiency.

RESULTS: Figure 1 shows temporal changes of the terminal voltage during galvanostatic electrolysis experiments for the CaCl$_2$-KCl molten salt containing various concentrations of CaO. Figure 2 shows the variation of cathode current efficiency to the initial concentration of CaO in the CaCl$_2$-KCl molten salt. The terminal voltage for the CaO concentration of 0 mass% corresponds a decomposition voltage of CaCl$_2$. The initial terminal voltage for the molten salt containing 0.5 – 2.0 mass% of CaO was lower than that for the molten salt containing 0 mass% of CaO and that increased with time, which means that anode reaction was an evolution of CO$_2$ or

formation of CO$_3^{2-}$ ion and CaO was consumed by electrolysis. The current efficiency was decreased with the increase of initial CaO content. After electrolysis, considerable amount of powdery carbon was confirmed in the molten salt whose initial CaO concentration was 1.0 mass% and 2.0 mass%. It is thus considered that the low current efficiency for the molten salt of high CaO content is due to a reduction of CO$_3^{2-}$ ion to C on cathode or reaction of metallic calcium in tin cathode with CO$_3^{2-}$ ion to form C.
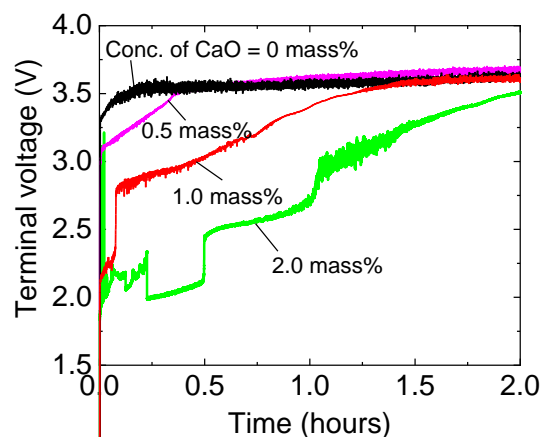

Fig. 1 Temporal change of the terminal voltage during electrolysis for the CaCl$_2$-KCl molten salt containing various concentration of CaO at 1000 K.
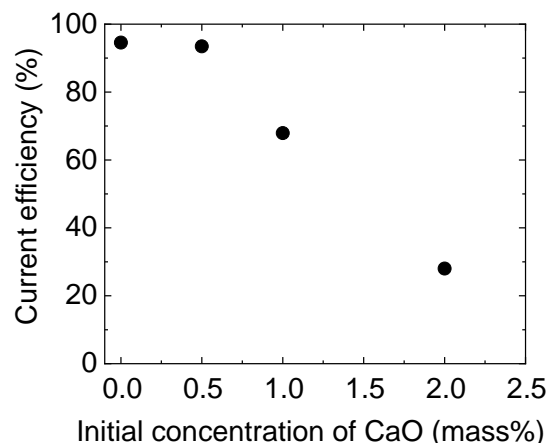

Fig. 2 Variation of cathode current efficiency to the initial concentration of CaO in the CaCl$_2$-KCl molten salt.

REFERENCE:
[1] J.J.Lukasko and J.E.Murphy: Report of Investigations (1990) RI9315.

Development of Mössbauer Spectroscopy for Various Isotopes

S. Kitao[1], M. Kobayashi[1], T. Kubota[1], M. Saito[1], R. Masuda[1], H. Ishibashi[2], S. Hosokawa[2] and M. Seto[1]

[1]*Research Reactor Institute, Kyoto University*
[2]*Graduate School of Science, Kyoto University*

INTRODUCTION:

The Mössbauer spectroscopy is one of the most powerful methods for investigation of electronic states, magnetic properties, chemical properties, and so on. A remarkable feature of this method is to extract the information of the specific isotope. This feature is effective to understand the essential properties of the materials, even with complex components. However, this method has a difficulty in obtaining and managing of the radioactive sources. Although about one hundred of Mössbauer energy levels are known, research activities in Mössbauer studies so far are quite limited, except ^{57}Fe and ^{119}Sn. It is partly because commercially available sources at present are only ^{57}Co and ^{119m}Sn for the Mössbauer spectroscopy of ^{57}Fe and ^{119}Sn, respectively.

On the contrary, at the Kyoto University Reactor(KUR), various short-lived isotopes can be obtained by neutron irradiation. We have already been performing Mössbauer spectroscopy of some isotopes, such as ^{125}Te, ^{129}I, ^{197}Au, by obtaining ^{125m}Te, ^{129}Te or ^{129m}Te, ^{197}Pt, respectively. Moreover, complementary short-lived isotopes can be produced by high-energy γ-ray irradiation at the electron linear accelerator(KUR-LINAC). The main purpose of this research is to increase the number of applicable Mössbauer spectroscopy by producing effective Mössbauer sources to apply various researches.
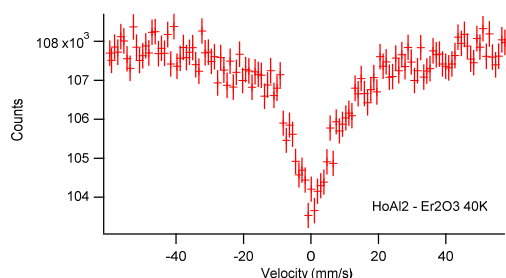

Fig. 1. ^{166}Er-Mössbauer spectrum of Er_2O_3 at 40K using ^{166}Ho source in $HoAl_2$ irradiated at KUR.

EXPERIMENTS AND RESULTS:

(1)^{166}Er Mössbauer spectroscopy

The 80.56keV level of ^{166}Er is known as one of useful levels for Er-Mössbauer spectroscopy. ^{166}Ho with a half-life of 26.8 hours can be used as a Mössbauer source. It is obtainable by neutron irradiation of natural Ho, which has 100% abundance of ^{165}Ho. One of candidates for the source material is $HoAl_2$[1]. A $HoAl_2$ was synthesized by arc-melting of Ho and Al metals. The neutron irradiation was performed by pneumatic tube(Pn)

for 5 minutes at 1MW operation of KUR. The 80.56keV γ-rays from ^{166}Ho source are well resolved by using a $CeBr_3$ scintillation counter. The ^{166}Er-Mössbauer spectrum of Er_2O_3 at the temperature of 40K by using ^{166}HoAl$_2$ source is shown in Fig. 1. The obtained spectra shows expected single-line spectrum. This proved the effectiveness of the ^{166}Er-Mössbauer spectroscopy by using thus obtained source. Since $HoAl_2$ shows ferromagnetic order at 27K, the $HoAl_2$ source should not be used at the temperature of lower than about 40K.

(2) ^{161}Dy Mössbauer spectroscopy

The 25.5keV level of ^{161}Dy is known as the most useful level for Dy-Mössbauer spectroscopy. As for the Mössbauer source, ^{161}Tb with a half-life of 6.88days is effectively usable. Since ^{161}Gd becomes ^{161}Tb in β-decay process with a half-life of 3.7 minutes, ^{161}Tb source is obtainable by neutron irradiation of ^{160}Gd. Since natural Gd contains 21.86% abundance of ^{160}Gd, natural Gd is usable by waiting a few days for decay of a by-product of ^{159}Gd with a half-life of 18.48 hours. A Gd-Mg alloy is used as a source material[2]. The neutron irradiation was performed by Pn for 1 hour at 5MW operation of KUR. The expected ^{161}Dy Mössbauer spectra were obtained successfully by using a Xe proportional counter.

Alternatively, ^{161}Tb can be produced through (γ, p) reaction by high-energy γ-ray irradiation of ^{162}Dy at KUR-LINAC. The γ-rays are produced by electron irradiation of water-cooled Pt converter. In use of natural Dy, some by-products are inevitable. For an attempt, we obtained a ^{161}Tb source by irradiation of a Dy metal using KUR-LINAC for 3 days. A Ge solid state detector is used to resolve the 25.5keV γ-rays. The ^{161}Dy-Mössbauer spectrum of DyF_3 at room temperature using ^{161}Tb source in Dy metal is shown in Fig. 2. Since expected spectrum was obtained, the results shows the effectiveness of this method.
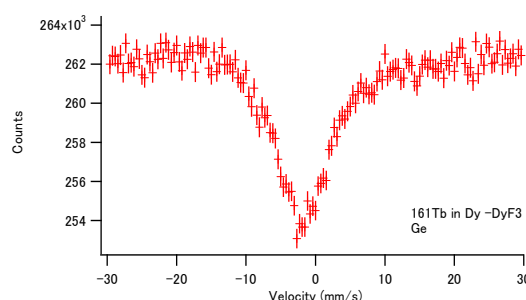

Fig. 2. ^{161}Dy-Mössbauer spectrum of DyF_3 at room temperature using ^{161}Tb source in Dy metal obtained at KUR-LINAC.

REFERENCES:

[1] R. L. Cohen and J. H. Wernick, Phys. Rev. **134** (1964) B503.
[2] G. J. Bowden, D. St. P. Bunbury, J. M. Williams, Proc. Phys. Soc. **916** (1967) 12.

Y. Kobayashi, Mariola Kadziołka-Gaweł[1], Damian Plażuk[1] and M. Seto

Institute for Integrated Radiation and Nuclear Science, Kyoto University
[1]Department of Organic Chemistry, Faculty of Chemistry, University of Łódź, Poland

INTRODUCTION: Organogold complexes have attracted considerable interest in the last decades mainly due to their rich structural chemistry, involving Au-Au interactions (aurophilicity), luminescent properties, catalytic and biological activity. Gold(I) complexes of the type L-Au-X are known to form dimers, oligomers or polymers. In some cases, these complexes undergo ligands scrambling leading to two new ionic gold(I) species L_2Au and AuX_2. Among a variety of such complexes special attention has been paid to gold(I) acetylides [1]. Some Au acetylides which have COC≡CAu structure cause ligands scrambling, but which have C≡CAu structure do not cause ligands scrambling. It is considered that this difference comes from the steric structure of the complexes. However, it is also said that the Au-Au bonding in the oligomer and the electronic state of Au cause the difference. We measured ^{197}Au Mossbauer spectra of Au acetylides to elucidate origin of the ligands scrambling.

EXPERIMENTS: Three Au acetylides were synthesized: #1: (FcCCAuPEt$_3$), #2: ((FcCOCC)$_2$AuAu(PEt$_3$)$_2$) and #3: (FcCOCCAuPEt$_3$) [2,3]. The detailed structures of these complexes were studied by X-ray diffraction and ^{31}P{^{1}H} NMR.

^{197}Au Mössbauer measurement was conducted using a constant-acceleration spectrometer with a NaI scintillation counter. The ^{197}Au γ-ray source (77.3 keV) was obtained from ^{197}Pt (half-life; 18.3 hrs) generated by irradiation of neutron to 98%-enriched ^{196}Pt metal foil using KUR. The γ-ray source and samples were cooled to 16 K, and the spectra were recorded in a transmission geometry. The isomer shift value of a gold foil was referenced to 0 mm/s.

RESULTS: Figure 1 shows ^{197}Au Mössbauer spectra of the Au acetylides. The amount of sample #3 was less than other samples, thus the absorption is small, and the distortion of the background line is larger than other spectra. The spectrum of #2 contains two components which relate to two different Au local surroundings. The spectra of #1 and #3 shows simple doublet. The values of isomer shift (IS) and quadrupole splitting (QS) are typical for AuL$_2$ type complexes [4]. If there is strong interaction between Au atoms in adjacent complexes, the IS values and QS values become near the values of four-coordinated Au atoms, which is smaller than typical values of AuL$_2$. However, such decreases of IS and QS are not observed. This result shows that the strong interaction between Au atoms do not exist. The difference of the ligands scrambling is not caused by the electronic state of Au.

On X-ray diffraction study, the formation of wire-like structures on COC≡CAu complexes. This structure is commonly on ligands-scrambling complexes. The steric structure is main factor of the ligands scrambling on these Au acetylides.
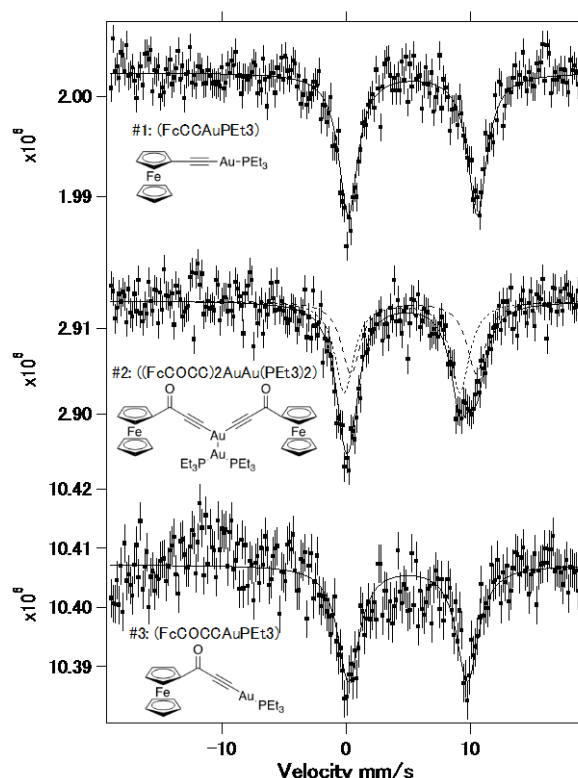

Fig. 1 ^{197}Au Mössbauer spectra of the Au acetylides at 16K.

REFERENCES:
[1] J. Carlos Lima and L. Rodríguez, *Chemical Society Reviews*, **40** (2011) 5442-5456.
[2] R. Flamholc, D. Plazuk, J. Zakrzewski, R. Métivier, K. Nakatani, A. Makal and K. Woźniak, *RSC Advances*, **4** (2014) 31594-31601.
[3] D. Plazuk and J. Zakrzewski, *Journal of Organometallic Chemistry*, **694** (2009) 1802-1806.
[4] G. J. Long, in *Mössbauer spectroscopy applied to inorganic chemistry*, Springer, 1984, pp. 7-26.

CO4-20 Complex Structure of Ions Coordinated with Hydrophilic Polymer 18. Application for Metaric Plating on Resin Surface (2)

A. Kawaguchi and Y. Morimoto

KURNS, Kyoto University

INTRODUCTION: We have reported interacted structures between iodine (polyiodide ions, I_n^{m-}, m, n: integer, $n \neq 1$) and polymers.[1] While polyiodide ions (and their counter-ions) are prepared as solutes in aqueous solution, they can be diffused into various polymeric matrix. Such structures and procedures are expected to introduce novel functionality and wide applications to polymeric materials with easy operation.[2]

For some hydrophilic polymers, diffusion of polyiodide from their aqueous solutions advances very quickly; since, in some matrix such as polyamide-6 (PA6), ionic diffusion into crystallite region or "diffusion-induced" orientation are also observed during doping operation at room temperature, as phenomena, iodine-doped polymers can be regarded as "pseudo solvents" for ionic diffusion.[3,4] These results suggest that coordination between iodine and polymers is dynamic and pliable and activated process and that previous existence of polyiodide ion drastically enhances posterior ionic diffusion in polymers. Such posterior diffusion means can be applied for functionalization for matrices with arbitrary shape or size, ocasionally, beyond hydrophobicity.

EXPERIMENTS: Samples are industrial products of micron-sized particles, which designed for ACF (anisotropic conduction film) or spacer with 2 or 5 mm diameters; they are synthesized as spherical particles of acryl resin showing fine-controlled dispersion of diameter. Some particles are products grafted with polystyrene (PS) on their spherical surface. [5]

These matrixes were "iodine-doped" by immersing in I_2-KI(aq) or I_2-NH_4I(aq) (0.1-3.0N) for more than one week. For secondary doping of Ag^+, each samples were immersed in $AgNO_3$(aq) (0.1-2.0M) for a few days. All operation were done at room temperature (c.a. 25℃).

For observation for section of spherical particles, transmission electron microscopy (TEM) was used for sliced matrices of the particles molded in epoxy resin.

RESULTS: One of noteworthy points is the samples have chemically hydrophobic materials of acrylic resin or grafted surface with PS, which powder actually show very low affinity with water or ordinary aqueous solutions. Nevertheless, process with the polyiodides aqueous solutions can easily introduce iodine on "(1st) iodine doping" and following Ag^+ ion on "secondary doping"; coloring with inner-diffused polyiodide (brown) or inner-precipitated AgI (light yellow) had been achieved in a few days or less. (Figure 1) And, TEM observation for the section of the sample after "Ag-secondary doping" with $AgNO_3$(aq) indicates that (1)precipitation of AgI grains advances in inner region of the micro particle, that (2)precipitation region is not exposed on surface of the particles; there is intermediate region between the surface of the spherical particles and region where AgI grains are grown up. (Figure 2) In the intermediate region, either polyiodide ions or precipitated AgI grains hardly exist. These results means that, (1)even for hydrophobic particle, polyiodide ions can be diffused from each aqueous solution, that (2)Ag^+ ion can be also diffused into the hydrophobic micro particle from the $AgNO_3$(aq), and that (3)AgI grains which have precipitated through diffusion of Ag^+ into the particles dissolute to external environment of the particles with advance of "Ag secondary doping". Such behavior is qualitatively similar to results in iodine doping and "Ag secondary doping" for other hydrophobic polymers: polyethylene (PE), polypropylene (PP), SERB elastomers, and "silicone rubber" tubes, previously reported.[6] While the intermediate region may be obstacle for plating on surface of the particles, it should be functionalization on the surface of hydrophobic materials.
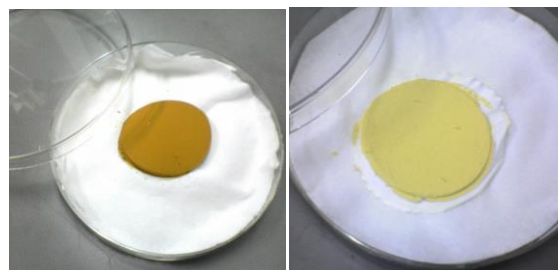

Fig.1: left: powder of micro particle after iodine-doping with polyiodide aqueous solution; right: next, the powder treated with $AgNO_3$(aq).
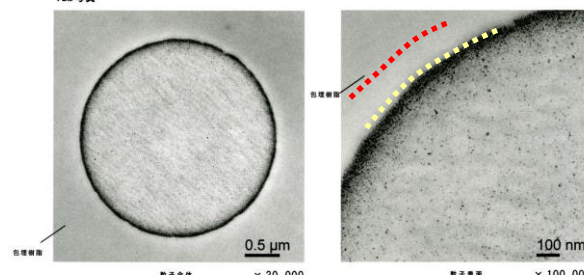

Fig.2: TEM observation for section of micro particle after "Ag-secondary doping" with $AgNO_3$(aq); either poly iodide ions or AgI exist hardly at intermediate region between spherical surface of micro particle (red, dotted line) and region of AgI precipitation (yellow, dotted line).

REFERENCES:

[1] A. Kawaguchi, Polymer, **35** (1994) 3797-3798.

[2] patent. JPN-5444559 (2014).

[3] KAWAGUCHI Akio, et.al., SPring-8 User Exp. Rep. **5** (2000A) (2000) 354-354.

[4] A.Kawaguchi, Polym.Prep.Jpn., **62** (2013) 5116-5117.

[5] "Projects for Practical Use from Innovation" sponsored by NEDO (2007-2009).

[6] A. Kawaguchi, et.al., KURRI Prog.Rep.2015 (2016) 79-79.

Study on Metal Surface Wettability Enhanced
by Radiation Induced Surface Activation

T. Hazuku, T. Ihara, R. Taguchi, S. Morooka[1], T. Miyoshi[1], H. Abe[2], S. Kano[2], T. Takamasa[3], D. Ito[4] and Y. Saito[4]

Tokyo University of Marine Science and Technology
[1]Waseda University
[2]The University of Tokyo
[3]National Institute of Technology, Toyama College
[4]Research Reactor Institute, Kyoto University

INTRODUCTION: A supercritical water-cooled reactor (SCWR) is one of the 4th generation nuclear reactors, which is based on the light water reactor technology and the thermal power generation technology [1]. The system is simple, compact and high thermal efficiency. Therefore, it is considered to have high safety and economic performance. On the other hand, radiation induced surface activation (RISA) phenomenon enhances metal surface wettability, boiling heat transfer and anticorrosive effects by the electrical interaction between the base material and the surface of oxidized film [2]. It implies that RISA phenomenon can contribute the much higher performance of SCWR and improve the safety features.

This study is mainly aimed at evaluations of the RISA effect on metal surface wettability at high temperatures and pressures.

EXPERIMENTS: Figure 1 shows a schematic diagram of the apparatus for contact angle measurement at high temperatures and pressures. A specimen was placed at the center of the pressure vessel. A water droplet was supplied on the specimen from the bottom. A high speed video camera with backlighting from a plate light photographed the water droplet on the specimen. The image of water droplet were recorded into a personal computer and the contact angle, an indicator of macroscopic wettability, was measured by image-processing. The stainless-304 and the PNC1520 which is considered as a potential material in the SCWR were used as the base test materials. Three kinds of specimens: (1) bare metals before gamma-ray irradiation, (2) bare metals after gamma-ray irradiation and (3) metals with an oxidized film surface after gamma-ray irradiation were prepared for measurements of contact angles. The oxidized film on the base metal was made by submerging the metal in an autoclave for 60 hours under a supercritical condition with temperature of 380ºC. The integrated irradiation dose of 60-Co gamma-ray was approximately 770 kGy.

RESULTS: Figure 2 compares the measured contact angles of water droplets on metals before gamma-ray irradiation, after gamma-ray irradiation and metals with oxidized film after gamma-ray irradiation. Although the surface wettability on the bare metals at room temperature conditions was drastically improved due to the RISA effect as is the results confirmed in the previous studies

[2], insignificant wettability improvement was confirmed under high temperatures over 290ºC even after gamma-ray irradiation.

On the other hand, it was confirmed that the surface wettability on the stainless-304 with oxidized film was improved due to RISA even under high temperatures. The wettability enhancement due to RISA effect is basically considered to be occurred by formation of hydrophilic domain like a hydroxyl on the oxidized film. The present results reveal that the formation efficiency of hydrophilic domain on the metals with the stable oxidized film may be much higher than that on the bare metals. The effect of oxidization of metals on RISA effect will be evaluated in detail in the future study.
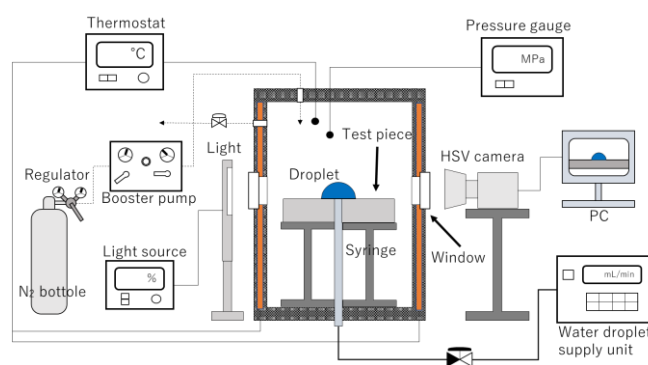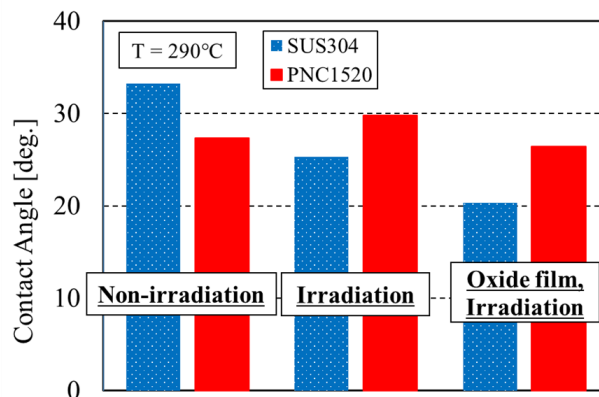

Fig. 1.   Apparatus

Fig. 2.   Comparison of measured contact angles

REFERENCES:
[1] Y. Oka and H. Mori, Supercritical pressure light water cooled reactor, Springer (2014).
[2] T. Takamasa, *et al.,* Development of high-performance nuclear reactor technology by radiation induced surface activation effect "Improvement of in-furnace heat transfer and corrosion prevention technology using surface active effect by irradiation, Journal of Atomic Energy Society of Japan, Vol.49, No.1 (2007) 45-50 [in Japanese].

CO4-22   Characterization of Heterogeneous Nanostructures Formed in Stainless Steel using Small-Angle Scattering

Y. Todaka, N. Adachi, Y. Oba[1] and M. Sugiyama[2]

Department of Mechanical Engineering, Toyohashi University of Technology
[1]Materials Sciences Research Center, Japan Atomic Energy Agency
[2]Institute for Integrated Radiation and Nuclear Science, Kyoto University

INTRODUCTION: Stainless steel is one of the most important materials and widely utilized as basic a structural material. Recent study has reported that heavy plastic deformation such as heavy cold rolling and high-pressure torsion (HPT) produce characteristic heterogeneous nanostructures composed of shear bands and nano-sized twins in the stainless steels [1]. These nanostructures can satisfy both high strength and high ductility. Furthermore, increases the strength of these nanostructured stainless steels increases with thermal ageing. However, the complicated heterogeneous nanostructures make it difficult to detect the origin of the strengthening using electron microscopes.

  Small-angle X-ray scattering (SAXS) is a powerful means to quantitatively characterize and compare the nanostructures between the samples. From the comparison of the samples before and after ageing, SAXS can analyze the change in the nanostructures. Therefore, we perform the SAXS measurements of the heterogeneous nanostructures formed in the stainless steels in this study.

EXPERIMENTS: A typical austenitic stainless steel JIS SUS316LN was chosen as the sample. HPT straining was conducted to form the heterogeneous nanostructures. SAXS measurements were performed using a SAXS instrument with Mo Kα radiation (Nano-viewer, RIGAKU) installed at the Institute for Integrated Radiation and Nuclear Science, Kyoto University. The characteristic X-ray emitted from Mo can penetrate steels. The sample-to-detector distance was 43 cm and 160 cm. During the SAXS measurements, the samples were put in vacuum to reduce the background scattering from air. A silver behenate and a glassy carbon were measured as the standard materials [2].

RESULTS: Fig. 1 shows SAXS profiles of the HPT-strained SUS316LN. Scattering intensities are clearly observed in the q range between 0.12 and 9 nm^{-1}. Here, q is the magnitude of the scattering vector. The intensity at around $q<1$ nm^{-1} shows difference. This indicates the change in the nanostructures roughly larger than 6 nm. It can be expected that significant increase by the
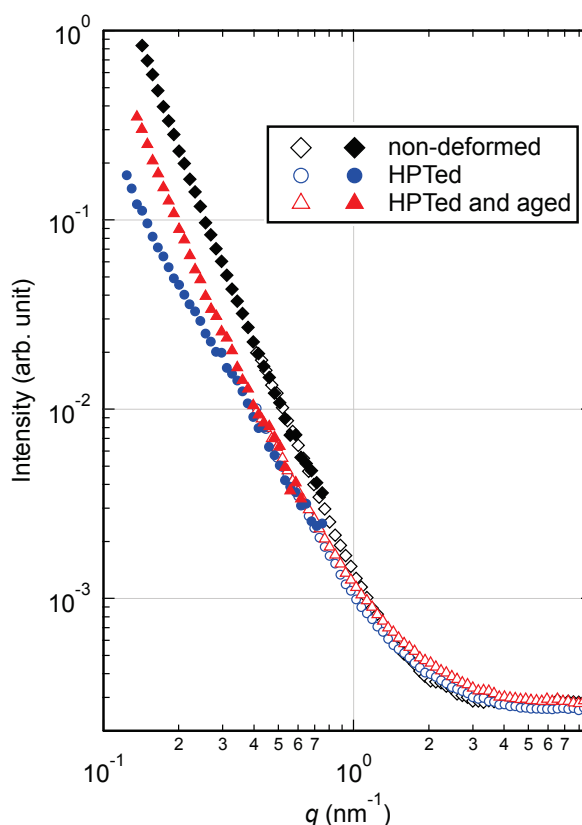

Fig. 1. SAXS profiles of the HPT-strained SUS316LN. Diamonds, triangles, and circles indicate the non-deformed sample, the HPT-strained sample, and the HPT-strained and aged sample, respectively.

thermal aging is given by nano-sized precipitates. The detailed structure of the nano-sized precipitate is still unknown. In order to analyze the chemical composition of the nanostructures, small-angle neutron scattering (SANS) experiments will be performed in the near future.

REFERENCES:
[1] H. Miura *et al.*, Scr. Mater., **133** (2017) 33-36.
[2] F. Zhang *et al.*, Metal. Mater. Trans. A, **41A** (2010) 1151-1158.

CO4-23 Research on Spin Density Wave in Mixed Anion Layered Compounds, $Sr_2VFeAsO_{3-\delta}$

Y. Tojo, T. Nakamura, H. Fujioka, M. Matoba, S. Kitao[1], M. Seto[1] and Y. Kamihara

Department of Applied Physics and Physico-Informatics, Faculty of Science and Technology, Keio University
[1]Research Reactor Institute, Kyoto University

INTRODUCTION: The discovery of high temperature iron-based superconductors in Mixed Anion Layered Compounds (MALC) [1] has triggered the search on the new superconducting materials. Much attention has been devoted to the newly developed superconductors with Fe-square lattices. In 2009, a family of superconducting layered iron pnictides was reported; $Ae_2MFePnO_3$ with a perovskite-type layered local structure of Ae_2MO_3, where Ae denotes an alkaline–earth metal, M denotes Sc, Ti, Cr, V or another transition metals, and Pn denotes P or As. [2] Among these compounds, $Sr_2VFeAsO_{3-\delta}$ has attracted attention as a practical superconducting material because of its large upper critical magnetic fields [3]. The crystal structure of $Sr_2VFeAsO_{3-\delta}$ is described as a tetragonal lattice with FeAs carrier conducting layers sandwiched by $Sr_2VO_{3-\delta}$ perovskite-related carrier-blocking layers. $Sr_2VFeAsO_{3-\delta}$, which has been reported with nominal chemical compositions, shows superconducting transitions at $T_c^{onset} \leq 37.2$ K [3] under ambient pressure and at $T_c^{onset} = 46.0$ K [4] under high pressure. In this work, we unveil magnetic phases and superconducting phase in an iron-based superconductor with a thick-blocking layer of a perovskite-related transition metal oxide, $Sr_2VFeAsO_{3-\delta}$.

EXPERIMENTS: Polycrystalline samples were prepared via a two-step solid-state reaction using dehydrated SrO, FeAs , V_2O_5, and V as starting materials. The phase purity and lattice constants of the resulting powders were examined by powder X-ray diffraction (XRD) (Rigaku; RINT2500Ultra18) using Cu Kα radiation from a rotating anode. ^{57}Fe Mössbauer spectra (MS) were obtained using conventional equipment with ^{57}Co source from 2.5 K to 300 K. [5] The ^{57}Fe MS were measured for δ = 0.124, 0.232, 0.237, 0.267, 0.509, and 0.631 samples. IS values of each sample are determined relative to that of α-Fe at room temperature.

RESULTS: Electronic and magnetic properties of ^{57}Fe in $Sr_2VFeAsO_{3-\delta}$. (a) Temperature (T) dependences of isomer shifts (IS), quadrupole splitting (QS) and full width at half maximum (FWHM) for $Sr_2VFeAsO_{3-\delta}$ samples with δ = 0.124 (open circle), 0.232 (open square), 0.237 (open triangles), 0.267 (closed triangles), 0.509 (red closed circles), and 0.631 (closed squares). The QS and FWHM values of the samples with δ = 0.267, 0.509, and 0.631 are written only when the spectrum is a doublet. The black lines in all plots indicate standard deviations. $\sqrt{<B_{int}^2>}$ are obtained from the distributions of the internal fields (B_{int}) of the samples with δ = 0.267, 0.509, and 0.631 exhibiting antiferromagnetic ordering of Fe
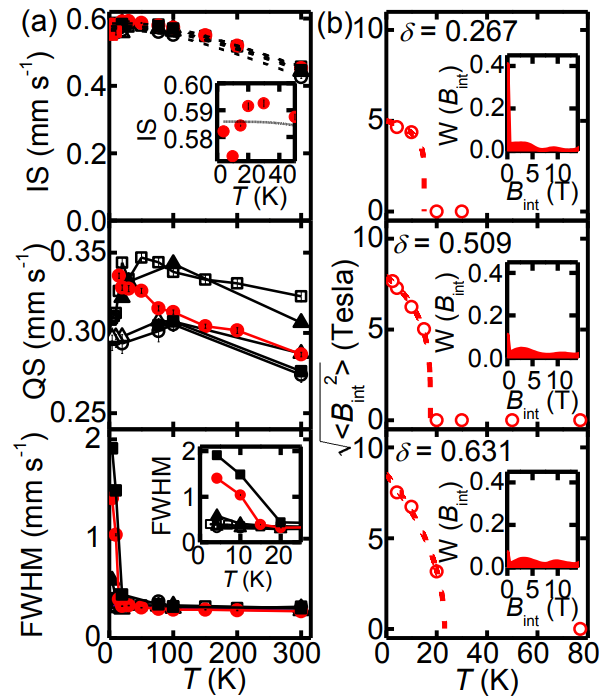

Fig. 1. Electronic and magnetic properties of ^{57}Fe in $Sr_2VFeAsO_{3-\delta}$. (a) Temperature (T) dependence of isomer shift (IS), quadruple splitting (QS), and full width half maxima (FWHM) for δ = 0.124 (open circle), 0.232 (open square), 0.237 (open triangles), 0.267 (closed triangles), 0.509 (red closed circles), and 0.631 (closed squares). (b) $\sqrt{<B_{int}^2>}$ versus T for δ = 0.267, 0.509, and 0.631. Insets show histograms of B_{int} distributions for each sample at 4.2 K. Figs are reprinted from Ref. 6.

sub-lattice at temperatures < Néel temperatures (T_N). The red dashed lines are fitted lines, obtained by the formula by

$$\sqrt{<B_{int}^2>} = B_0(1-\frac{T}{T_N})^{\alpha} \quad \text{for } 0 \leq T/T_N \leq 1$$

with α = 0.5. Details results and discussions have been reported in ref. 6.

REFERENCES:
[1] H. Hiramatsu and Y. Kamihara, in Transparent oxides as active electronic materials and their appliations, edited by H. Hosono and M. Hirano (CMC publishing, Tokyo, 2006), p. 71-93, Layered compounds (in Japanese).
[2] H. Ogino, *et al*, Supercond. Sci. Technol., **22** (2009) 085001.
[3] X. Zhu, *et al*, Phys. Rev. B **79**, 220512 (2009).
[4] H. Kotegawa, *et al*, J. Phys. Soc. Jpn., **78** (2009) 123707.
[5] S. Kitao, *et al*, J. Phys. Soc. Jpn., **77** (2008) 103706.
[6] Y. Tojo, *et al,* arXiv:1802 (2018) 03907.

Vacancy Migration Behavior in a CoCrFeMnNi High Entropy Alloy

K. Sugita, M. Mizuno, H. Araki, A. Yabuuchi[1] and A. Kinomura[1]

Graduate School of Engineering, Osaka University
[1]*Institute for Integrated Radiation and Nuclear Science, Kyoto University*

INTRODUCTION: The alloy design has been conventionally performed by choosing a base metal and adding suitable elements to achieve desired properties. Over the last decade, a new type of multicomponent alloys called as "high entropy alloys", which include equiatomic / near-equiatomic proportion of constituent elements, have been proposed by Yeh et al. [1-3]. They often show simple solid solution structures at high temperature due to high configurational entropy of mixing for a random solid solution. High entropy alloys have been reported to have the following promising properties of practical interest, such as high strength combined with ductility, high fracture toughness, excellent oxidation and corrosion resistance. "Sluggish diffusion" kinetics is believed to be a main contributor to these properties. Therefore it has also created fundamental interest for atomic diffusion in a multiprincipal element matrix, and the diffusion kinetics in high entropy alloys has been actively investigated by diffusion couple method and tracer-diffusion method.

In this work, we contribute to a debate about hypothetical sluggish diffusion phenomena in high entropy alloys by investigating the vacancy migration behavior in a CoCrFeMnNi alloy during the isochronal annealing after electron-irradiation.

EXPERIMENTS: Metal pieces of Co, Cr, Fe, Mn and Ni with 99.9% up purity were added together in equiatomic proportions to produce $Co_{20}Cr_{20}Fe_{20}Mn_{20}Ni_{20}$ alloy ingots by arc melting followed by homogenization at 1373 K for 24 h. $Fe_{40}Cr_{15}Ni_{45}$ alloy ingots were also prepared for comparison. The alloy ingots were cut into square plate specimens with dimensions of $10 \times 10 \times 0.5$ mm^3. The specimens were subjected to strain relief annealing at 1373K for 10 h and then rapidly cooled to prevent secondary phase precipitation and to stabilize single-phase FCC structures. The specimens in water flow were exposed to 8 MeV electron beam irradiation for 1 h in KURRI-LINAC. The irradiation damage was evaluated at $(1.3 - 1.8) \times 10^{-4}$ dpa. In order to investigate the thermal stability of vacancies, the electron irradiated specimens were subjected to the subsequent isochronal annealing for 1 at 373-593K.

Positron lifetime measurements were carried out by using a digital oscilloscope system with photomultiplier tubes mounted with BaF_2 scinitillators, having a time resolution (FWHM) of 180 ps. The positron lifetime measurements require data acquisition for approximately 12 hours with a Na-22 positron source of 0.6 MBq activity in order to acquire 3 million counts in the positron lifetime spectrum. The measured spectra were analyzed using the programs RESOLUTION and POSITRONFIT Extended.

RESULTS: Mean positron lifetime in the electron-irradiated CoCrFeMnNi and CrFeNi specimens after isochronal annealing is shown in Fig.1. The positron lifetime spectra of as-irradiated CoCrFeMnNi and CrFeNi specimens shows a clear splitting into two exponential components with the longer lifetime values of 185-195 ps. This indicates that a part of positrons are trapped by monovacancies and relatively small vacancy clusters produced during the electron beam irradiation. After the subsequent isochronal annealing, the mean positron lifetime is observed to decrease sharply around 473K. This can be attributed to the decrease in vacancy concentrations triggered by the free vacancy-migration. It demonstrates the vacancy migration enthalpy in the CoCrFeMnNi high entropy alloy is very similar to that in the CrFeNi alloy. These results indicates that the "'sluggish diffusion" hypothesis is not supported in a CoCrFeMnNi high entropy alloy at least in view of vacancy migration behavior.
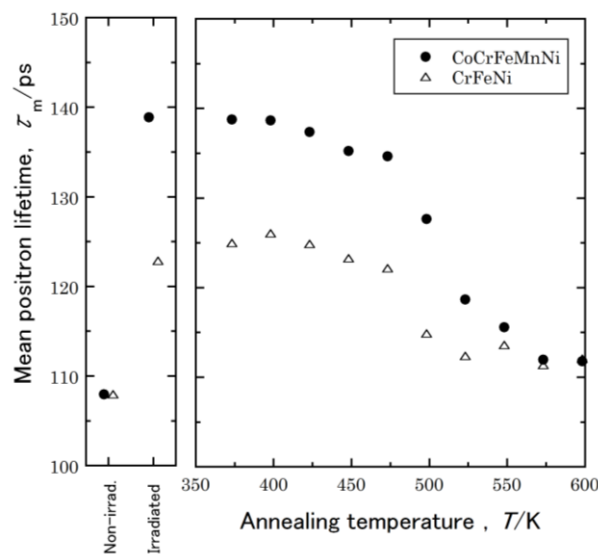

Fig. 1 Mean positron lifetime in the electron-irradiated CoCrFeMnNi and CrFeNi alloys after isochronal anneaing.

REFERENCES:
[1] C. Y. Hsu, J. W. Yeh, S. K. Chen, T. T. Shun: Metall. Mater. Trans. **35A**, (2004), 1465.
[2] J. W. Yeh, S. K. Chen, S. J. Lin, J. Y. Gan, T. S. Chin, T. T. Shun, C. H. Tsau, S. Y. Chang: Adv. Eng. Mater., **6** (2004) 299.
[3] J. W. Yeh: Ann. Chim. Sci. Mat., **31** (2006) 633.

Positron Age-MOmentum Correlation (AMOC) measurements on Gamma-ray Irradiated Polystyrene

H. Tsuchida[1,2], D. Ueda[2], S. Konishi[2] and Q. Xu[2]

[1]*Quantum Science and Engineering Center, Kyoto University*
[2]*Department of Nuclear Engineering, Kyoto University*
[3]*Institute for Integrated Radiation and Nuclear Science, Kyoto University*

INTRODUCTION: Studies on radiation damage in materials are of technical importance for developing radiation-resistant materials used in an irradiation environment [1,2]. In this work, we investigated radiation damage in polymers. The purpose of this study is to understand a fundamental nature of radical-related radiation damage. Gamma-ray irradiated polystyrene was analyzed using positron Age-MOmentum Correlation (AMOC) technique. The AMOC combines positron lifetime and annihilation gamma-ray Doppler-broadening spectroscopy by correlated measurements of the positron age and the Doppler shift of one of the annihilation quanta. In this analysis, we developed a new system, $\beta^+-\gamma$ coincidence-based AMOC.

EXPERIMENTS: The irradiation experiments were performed at Co-60 gamma-ray irradiation facility at KURNS. Polystyrene with a thickness of 2 mm was used as a sample. The sample was irradiated with the gamma-rays at two different doses of 30 and 300-kGy at room temperature. Position annihilation analysis was carried out at our facility, where we developed AMOC system combined with $\beta^+-\gamma$ coincidence positron lifetime spectroscopy. The positron source used was Ge-68.

RESULTS: Fig. 1 shows AMOC spectrum (correlation between the energy of annihilation gamma-rays and the positron lifetime) for the sample irradiated at dose of 300-kGy. Long-lifetime components (above 1 ns) correspond to positron annihilation characteristic on formation of positronium (Ps) in open volume defects of materials. Namely, self-annihilation of para-Ps has a lifetime of 0.12 ns, whereas pick-off annihilation of ortho-Ps has typically a lifetime of 0.5−5.0 ns.

Based on observed spectra, we obtained time dependent line-shape parameter *S*. Fig. 2 shows the results for the samples irradiated at two different doses of 30 and 300-kGy. The *S* parameter gradually decreases in the time range below 1 ns, in which self-annihilation of para-Ps mainly occurs. With increasing dose, the values of *S* are reduced. This reduction is attributed to the damage accumulation. In the result for the sample irradiated at 300-kGy, the *S* increases in the range above 1 ns, and becomes maximum around 3.5 ns. This result may be related to the pick-off annihilation of ortho-Ps originating from interactions with radical-related damage. To determine this observation, we will perform further research for identification of radical-related damage by electron spin resonance (ESR) method.
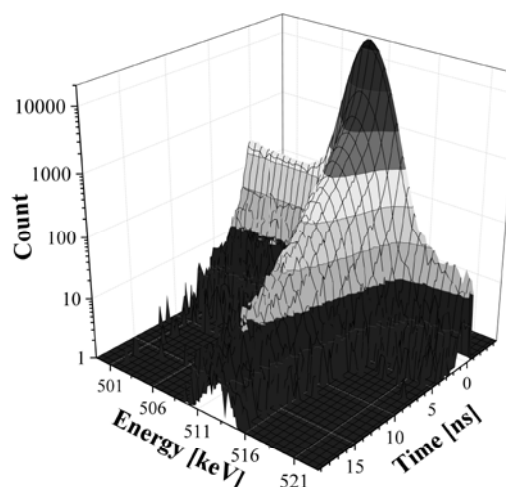

Fig. 1. AMOC spectrum for polystyrene irradiated with Co-60 gamma-rays at dose of 300-kGy.
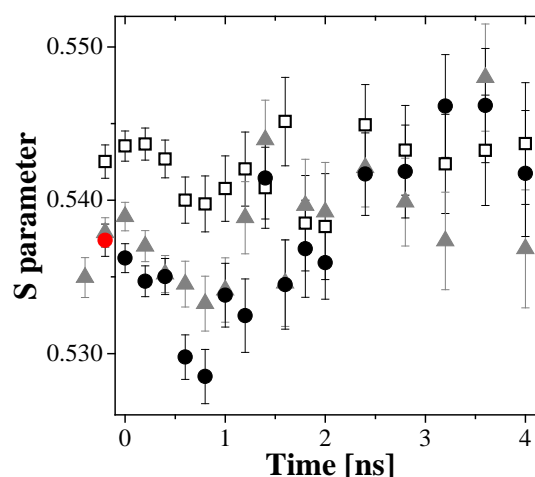

Fig. 2. Line-shape parameter *S* as a function of time (positron age) for gamma-ray irradiated polystyrene at various doses: □ un-irradiated, ▲ 30-kGy, and ● 300-kGy.

REFERENCES:
[1] H. Tsuchida *et al.*, Jpn. J. Appl. Phys. Conf. Proc., **2** (2014) 011103.
[2] H. Tsuchida *et al.*, Mater. Res. Express, **3** (2016) 055201.

Establishment of Mössbauer Spectroscopy on Rare Earth Er

H. Yokota, S. Jitsukawa, S. Nakamura[1], S. Kitao[2], Y. Kobayashi[2], M. Saito[3], R. Masuda[3] and M. Seto[2]

Graduate School of Science, Chiba University
[1]Department of Physics, TeikyoUniversity
[2]Research Reactor Institute, Kyoto University

INTRODUCTION: As the strong demands of the miniaturization of devices, controlling more than two order parameters at the same time is the key factor to open up the new possibility for designing the novel applications. Multiferroics are the most promising candidates for this usage since they possess more than two ferroic properties in the same phase [1-4]. Especially, cross-control of magnetization and polarization by electric and magnetic fields provides a great potential. In spite of their attractive properties, most of multiferroics exhibit their properties at low temperature, which make us difficult to realize the devices using multiferroics. Recent progress on thin film fabrications is changing this situation and now we are able to obtain material which cannot be realized as a bulk form. Hexagonal rare earth ferrites (h-REFeO$_3$), which we are interested in, are one of the examples and this series of materials are only obtained as thin film or nano particle form. In the case of bulk, orthorhombic perovskite structure becomes a stable state. Therefore not so many reports on h-REFeO$_3$ has have been reported so far. Recently, room temperature multiferroic properties have been reported in hexagonal LuFeO$_3$ thin film and this class of materials has been receiving an attention [5-9]. We succeeded to fabricate h-ErFeO$_3$ thin film by using a pulsed laser deposition technique and investigated its physical properties by various methods. We confirmed that h-ErFeO$_3$ thin film was epitaxially grown and it exhibits ferroelectricity at room temperature. The superconducting quantum interference device (SQUID) measurements disclosed that the magnetization shows the discrepancy between zero field cooling (ZFC) and field cooling (FC) processes under a weak magnetic field. Below the magnetic transition temperature of 120 K, it shows an apparent magnetic hysteresis loop indicating the weak ferromagnetic property of h-ErFeO$_3$ thin film. The Mössbauer spectroscopy clarified that the Fe ions are in the high-spin Fe^{3+} state and we proposed a possible magnetic structure of Fe ion[10]. Although our previous experiments elucidated ferroelectric and weak ferromagnetic properties of h-ErFeO$_3$ thin film, there are still some ambiguities of this material. The Mössbauer spectroscopy is very powerful technique and provides abundant knowledge about a magnetic and electronic state concerning the targeted nuclides in compounds. In spite of its efficiency, most of the Mössbauer studies are limited on ^{57}Fe or ^{119}Sn ion and not many reports exist on rare earth ions. The purpose of our study is to establish the Mössbauer spectroscopy on rare earth Er ion and apply this technique on h-ErFeO$_3$ thin film.

EXPERIMENTS: HoAl$_2$ was irradiated for 5 minutes at 1MW power at KUR and used as γ-source. Er$_2$O$_3$ powder and h-ErFeO3 thin films were used as samples and the measurements were carried out at 40 K. CeBr$_3$ Scintillation counter was used as a detector.

RESULTS: Figure 1 shows the Mössbauer spectrum of Er$_2$O$_3$ powder. It exhibits a typical paramagnetic behavior. It suggests that we succeeded to measure the Mössbauer spectrum for rare earth Er element. On the other hand, our trial on h-ErFeO$_3$ thin films is very difficult to obtain enough intensity an SN ratio to discuss about its magnetic properties. Further trial using a stronger γ-intensity or Er radioactive enrich sample is needed.
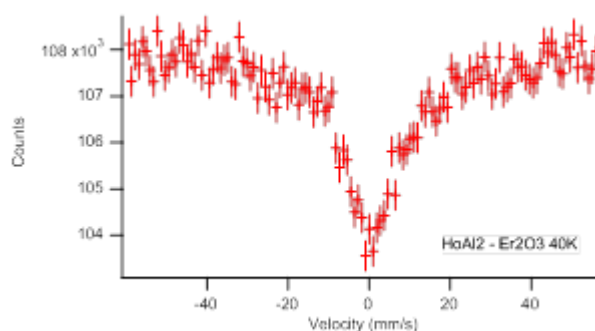

Fig. 1.   Mössbauer spectrum of Er$_2$O$_3$ powder measured at 40 K

REFERENCES:
[1] H. Schmid, Ferroelectrics **162** (1994) 317-338 .
[2] T. Kimura, T. Goto, H. Shintani, K. Ishizaka, T. Arima, and Y. Tokura, Nature **426** (2003) 55.
[3] Fiebig, J. Phys. D: Appl. Phys., **38** (2005) R123-R152 .
[4] G. Catalan and James F. Scott, Adv. Mater., **21** (2009) 2463–2485 .
[5] A. R. Akbashev, A. S. Semisalova, N. S. Perov, and A. R. Kaul, Appl. Phys. Lett., **99 (2011)** 122502.
[6] Y. K. Jeong, J.-H. Lee, S.-J. Ahn, S.-W. Song, H. M. Jang, H. Chio, and J. F. Scott, J. Ame. Chem. Soc., **134** (2012) 1450 .
[7] Y. K. Jeong, J.-H. Lee, S.-J. Ahn, and H. M. Jang, Chem. Mat., **24** (2012) 2426 .
[8] H. Iida, T. Koizumi, Y. Uesu, K. Kohn, N. Ikeda, S. Mori, R. Haumont, P.-E. Janolin, J-M. Kiat, M. Fukunaga, and Y. Noda, J. Phys. Soc. Jpn., **81** (2012) 024719.
[9] W. Wang, J. Zhao, W. Wang, Z. Gai, N. Balke, M. Chi, H. N. Lee,W. Tian, L. Zhu, X. Cheng, D. J. Keavney, J. Yi, T. Z.Ward, Paul C. Snijders, H. M. Christen, W. Wu, J. Shen, and X. Xu, Phys. Rev. Lett., **110** (2013) 237601 .
[10]   H. Yokota, T. Nozue, S. Nakamura, H. Hojo, M. Fu-kunaga, P. E. Janolin, K. M. Kiat and A. Fuwa, Phys. Rev. B, **92** (2015) 054101.

Dose Response and Mechanism of Radiophotoluminescence Phenomenon Induced by γ-ray Irradiation in Cu-doped Glass

R. Hashikawa, Y. Fujii, A. Kinomura[1], T. Saito[1],
A. Okada[2], T. Wakasugi[2] and K. Kadono[2]
*Graduate School of Science and Technology,
Kyoto Institute of Technology*

[1]*Institute for Integrated Radiation and Nuclear Science,
Kyoto University*

[2]*Faculty of Materials Science and Engineering,
Kyoto Institute of Technology*

INTRODUCTION: Radiophotoluminescence is a phenomenon in which photoluminescence is induced in materials by the exposure to ionizing radiation. It is well known that Ag-activated phosphate glass exhibits strong radiophotoluminescence, in which the intensity of the induced luminescence is proportional to the absorbed dose. Then the Ag-activated phosphate glass is practically used as a personal dosimeter [1]. However, there are few studies on the radiophotoluminescence behaviors of glasses other than the Ag-activated glass [2]. We have been interested to the luminescence properties of Cu-doped materials and explored new glasses exhibiting radiophotoluminescence with high performance. Here, we present the photoluminescence in a Cu-doped aluminoborosilicate glass induced by the γ-ray irradiation and the mechanism for the enhancement of the luminescence.
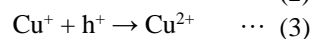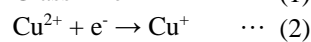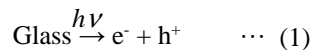
EXPERIMENTS: A Glass with the composition, $25Na_2O \cdot 25Al_2O_3 \cdot 10B_2O_3 \cdot 40SiO_2$ (mol%) (ABS25), was prepared from raw materials, $NaNO_3$, Al_2O_3, B_2O_3, SiO_2, CuO, by the conventional melting-cooling method. The batch mixtures with CuO were melted at 1600°C for two hours using a Pt crucible. The concentration of Cu was 0.005 mol% for 100 mol% of glass. The prepared glass was annealed at 660°C and cut to the size of 15 x 15 mm^2 and 1 mm in thickness. Both sides of the glass were optically polished.

The γ-ray irradiation experiments were performed with 60Co γ-ray at the Co-60 Gamma-ray Irradiation Facility at Institute for Integrated Radiation and Nuclear Science, Kyoto University. The irradiation dose was represented as absorbed dose for water.

RESULTS: Figure 1 shows the photoluminescence spectra of the 0.005 mol% Cu-doped glass irradiated by the γ-ray with various dose. Increasing the absorbed dose, the intensity of the luminescence band at 2.5 eV (500 nm), assigned to the $3d^94s^1 \rightarrow 3d^{10}$ transition, was increased. Figure 2 shows the relationship of the integrated intensity of the luminescence against the absorption dose. The excellent linearity between 40 Gy and 1.1×10^3 Gy of the absorbed dose was observed. At the absorbed dose below 40 Gy and above 1.1×10^3 Gy, the luminescence intensities were deviated to higher and lower sides of the line, respectively.

It is expected that the exposure of the Cu-doped glass to the ionizing radiation induces the fol-

lowing reactions in it. The eq. (1) shows the generation of electron-hole pairs. The generated electrons and holes are trapped at Cu^{2+} and Cu^+ ions through eq. (2) and (3), respectively.

$$Glass \xrightarrow{h\nu} e^- + h^+ \qquad \cdots (1)$$
$$Cu^{2+} + e^- \rightarrow Cu^+ \qquad \cdots (2)$$
$$Cu^+ + h^+ \rightarrow Cu^{2+} \qquad \cdots (3)$$

When the absorbed dose is small, the effect of eq. (3) suppressing the increase of the amount of Cu^+ can not be negligible. Then the intensity of the photoluminescence was deviated to the higher side from the line. On the other hand, increasing the absorption dose beyond 1.1×10^3 Gy, the reaction of the electron capture expressed by eq. (2) reached the saturation. Then, the intensity of the photoluminescence deviated to the lower side from the line.

More quantitative investigations relating the absorbed does, and the amount of the generated electron-hole pairs, Cu^+, and Cu^{2+} are planned in the near future.
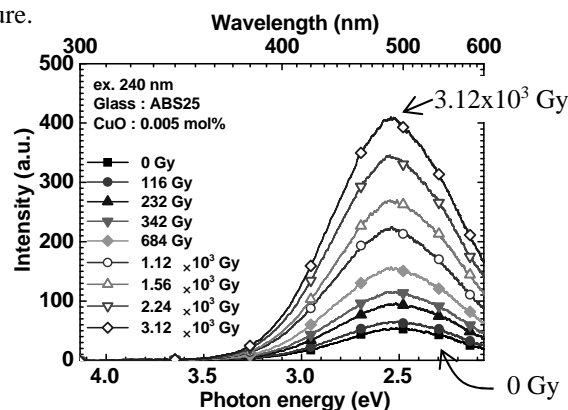

Fig. 1. Emission spectra of ABS25 doped with 0.005 mol% CuO at various absorbed doses.
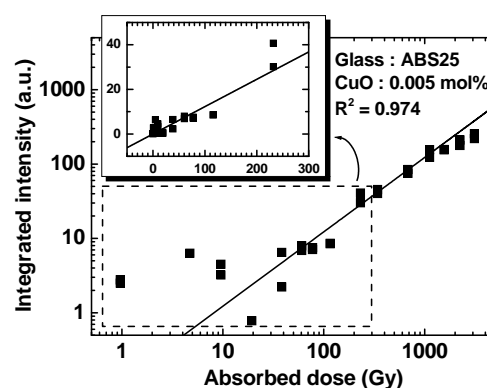

Fig. 2. Plot of integrated intensity of emission spectra versus the absorbed dose of ABS25 doped with 0.005 mol% CuO.

REFERENCES:
[1] Y. Miyamoto *et al.*, Radiat. Meas., **46** (2011) 1480-1483.
[2] R. K. Parajuli *et al.*, Key. Eng. Mat., **698** (2016) 163-170.